Received: 9 December 2021 | Revised: 5 July 2022 | Accepted: 5 July 2022

DOI: 10.1002/nme.7074

RESEARCH ARTICLE

WILEY

Shape optimization for the mitigation of coastal erosion via porous shallow water equations

Luka Schlegel | **Volker Schulz**

Department of Mathematics, University of Trier, Trier, Germany

Correspondence
Luka Schlegel, Department of Mathematics, University of Trier, Trier, Germany.
Email: schlegel@uni-trier.de

Funding information
Deutsche Forschungsgemeinschaft, Grant/Award Number: SPP 1962

Abstract

Coastal erosion describes the displacement of land caused by destructive sea waves, currents, or tides. Major efforts have been made to mitigate these effects using groynes, breakwaters, and various other structures. We address this problem by applying shape optimization techniques on the obstacles. We model the propagation of waves toward the coastline using two-dimensional porous shallow water equations with artificial viscosity. The obstacle's shape, which is assumed to be permeable, is optimized over an appropriate cost function to minimize the height and velocities of water waves along the shore, without relying on a finite-dimensional design space, but based on shape calculus.

KEYWORDS

adjoint methods, coastal erosion, numerical methods, obstacle problem, porous shallow water equations, shape optimization

1 | INTRODUCTION

Coastal erosion describes the displacement of land caused by destructive sea waves, currents or tides. Major efforts have been made to mitigate these effects using groynes, breakwaters and various other structures. Among experimental set-ups to model the propagation of waves toward a shore and to find optimal wave-breaking obstacles, the focus has turned toward numerical simulations due to the continuously increasing computational performance. Calculating optimal shapes for various problems is a vital field, combining several areas of research. This article builds up on the monographs[1-3] to perform free-form shape optimization. In addition, we strongly orientate on References 4 and 5 that use the Lagrangian approach for shape optimization, that is, calculating state, adjoint, and the deformation of the mesh via the volume form of the shape derivative assembled on the right-hand side of the linear elasticity equation, as Riesz representative of the shape derivative.

Essential contributions to the field of numerical coastal protection have been made for steady[6-8] and unsteady[9-11] descriptions of propagating waves. In this article, we select one of the most widely applied system of wave equations. We describe the hydrodynamics by the set of Saint-Venant or better known as shallow water equations (SWE), that originate from the famous Navier–Stokes equations by depth-integrating, based on the assumption that horizontal length-scales are much larger than vertical ones.[12] To model a permeable obstacle, which can be exemplifying interpreted as a geotextile tube, a porosity parameter is introduced. Porous SWE models are being paid increasing attention throughout the last decade, mostly because its ability to perform large-scale urban flood modeling.[13] Over the years a variety of models have been introduced differing in terms of conceptual, mathematical, and numerical aspects.[14-16] Our model mainly builds up on Reference 14, such that we are dealing with a single, depth-independent porosity parameter in the definition of the

SWE. In addition, we restrict ourself to isotropic porosity effects, such that the parameter cannot account for directional effects, which forms a legitimate assumption for a geotextile obstacle.

We would like to highlight that porous SWE have been modeled mainly by techniques relying on constant cell approximations via finite volume schemes. In this article, we calculate and derive numerical solutions to porous SWE by high-order discontinuous Galerkin (DG) methods. In this setting, artificial viscosity is introduced to counter possible oscillations that can appear around a shock location and discretized using a symmetric interior penalty discontinuous Galerkin (SIP-DG).[17] To deal with numerical difficulties that arise due to the discontinuous material coefficient, we extend the notion of a well-balanced DG scheme for classical SWE with discontinuous sediment[18] to porous, diffusive and two-dimensional SWE. In addition, it is noteworthy, that porous SWE have not been investigated in any kind of optimization yet, such that we first formulate adjoint and shape derivative for this set of equations and provide an algorithmic handle to this.

The article is structured as follows: In Section 2, we formulate the PDE-constrained optimization problem. In Section 3, we derive the necessary tools to solve this problem, by deriving adjoint equations and the shape derivative in volume form. The final part, Section 4, will present numerical techniques and applications for a sample mesh such as a representative mesh for a real coastal section.

2 | PROBLEM FORMULATION

Suppose we are given an open domain $\Omega \subset \mathbb{R}^2$, which is split into the disjoint sets $\tilde{\Omega}, D \subset \Omega$ such that $\tilde{\Omega} \cup D \cup \Gamma_3 = \Omega$ and $\Gamma_1 \cup \Gamma_2 = \partial\Omega (=: \Gamma_{\text{out}})$. We assume the variable, interior boundary and the fixed outer $\partial\Omega$ to be at least Lipschitz. One simple example of such kind is visualized below in Figure 1.

On this domain, we model water wave and velocity fields as the solution to porous SWE with artificial viscosity. We interpret $\Gamma_1, \Gamma_2, \Gamma_3$ as coastline, open sea, and obstacle boundary and solve on $\Omega \times (0, T)$

$$\partial_t(\phi U) + \nabla \cdot (\phi F(U)) - \nabla \cdot (G(f(\phi, \mu))\nabla \hat{U}) = \phi S(U) + S_\phi(U), \tag{1}$$

where we are given the SWE in vector notation with flux matrix

$$F(U) = \begin{pmatrix} \vec{Q} \\ \frac{\vec{Q}}{H} \otimes \vec{Q} + \frac{1}{2} g H^2 \mathbf{I}_2 \end{pmatrix} = \begin{pmatrix} Hu & vH \\ Hu^2 + \frac{1}{2} g H^2 & Huv \\ Huv & Hv^2 + \frac{1}{2} g H^2 \end{pmatrix} \tag{2}$$

for identity matrix $\mathbf{I}_2 \in \mathbb{R}^{2\times 2}$ and solution $U : \Omega \times (0, T) \to \mathbb{R} \times \mathbb{R}^2$, where for simplicity the domain and time-dependent components are denoted by $U = (H, \vec{Q}) = (H, Hu, Hv)$, with H being the water height and Hu, Hv the weighted horizontal and vertical discharge or velocity. For notational ease, we set $\hat{U} = (H + z, \vec{Q})$ for constant sediment height $z : \Omega \times (0, T) \to \mathbb{R}$. The porosity is a scalar function $\phi : \Omega \times (0, T) \to (0, 1]$ representing the respective portion of space that is available to the flow. We define

$$\phi \equiv \begin{cases} \phi_1 = \text{const. in } \tilde{\Omega} \times (0, T), \\ \phi_2 = \text{const. in } D \times (0, T). \end{cases} \tag{3}$$

The setting can be taken from Figure 2, where the region with varying porosity factor on D is exemplifying highlighted in gray.

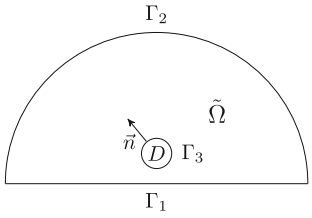

FIGURE 1 Illustrative domain Ω with initial circled obstacle D and boundaries Γ_1, Γ_2, and Γ_3

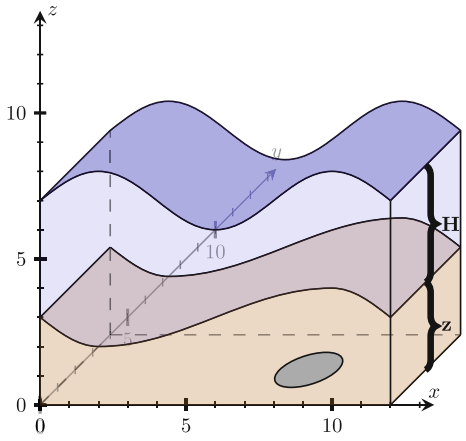

FIGURE 2 Cross-section for identification of wave height H, sediment height z, and material coefficient

We define the first source term in (1) as

$$S(U) = \begin{pmatrix} 0 \\ -gH\frac{\partial z}{\partial x} \\ -gH\frac{\partial z}{\partial y} \end{pmatrix}, \tag{4}$$

responding to variations in the bed slope. In addition, the parameter g represents the gravitational acceleration. The second source term in (1) corresponds to variations in the porosity coefficient and is chosen as[14]

$$S_\phi(U) = \begin{pmatrix} 0 \\ g\frac{H^2}{2}\frac{\partial \phi}{\partial x} \\ g\frac{H^2}{2}\frac{\partial \phi}{\partial y} \end{pmatrix}. \tag{5}$$

For the SWE, we employ outer boundary conditions as rigid-wall and open sea boundary conditions for Γ_1 and Γ_2 as

$$\begin{aligned} &\vec{Q}\cdot\vec{n} = 0,\ \nabla(H+z)\cdot\vec{n} = 0,\ \nabla Q_1\cdot\vec{n} = 0,\ \nabla Q_2\cdot\vec{n} = 0, && \text{on } \Gamma_1\times(0,T), \\ &H = H_1,\ \nabla Q_1\cdot\vec{n} = 0,\ \nabla Q_2\cdot\vec{n} = 0, && \text{on } \Gamma_2\times(0,T), \end{aligned} \tag{6}$$

and transmissive interface conditions on $\Gamma_3\times(0,T)$ for the continuity of the state

$$[\![H+z]\!] = 0, \tag{7}$$
$$[\![Q_1]\!] = 0, \tag{8}$$
$$[\![Q_2]\!] = 0, \tag{9}$$

the diffusive flux

$$[\![\nabla(H+z)\cdot\vec{n}]\!] = 0, \tag{10}$$
$$[\![\phi\nabla(Q_1)\cdot\vec{n}]\!] = 0, \tag{11}$$
$$[\![\phi\nabla(Q_2)\cdot\vec{n}]\!] = 0, \tag{12}$$

and the advective flux

$$[\![\phi F(U)\cdot\vec{n}]\!] = 0, \tag{13}$$

that is,

$$[\![\phi\vec{Q}\cdot\vec{n}]\!] = 0, \tag{14}$$
$$[\![\{\phi Q_1^2/H + 1/2g\phi H^2; \phi Q_1 Q_2/H\}\cdot\vec{n}]\!] = 0, \tag{15}$$

$$[\![\{\phi Q_1 Q_2/H; \phi Q_2^2/H + 1/2g\phi H^2\} \cdot \vec{n}]\!] = 0, \tag{16}$$

for jump symbol on the interface Γ_3 defined by $[\![H]\!] := H\big|_{\tilde{\Omega}} - H\big|_{\tilde{D}}$. In addition, we prescribe to be determined initial conditions on $\Omega \times \{0\}$ as

$$U = U_0. \tag{17}$$

Remark 1. To prevent shocks or discontinuities and associated local oscillations that can appear in the original formulation of the hyperbolic SWE even for continuous data in finite time, diffusive terms are added in (1) such that we obtain a set of fully parabolic equations. We control the amount of added diffusion by diagonal matrix $G(f(\phi,\mu)) = \sum_{i=1}^{n} e_i^T f(\phi,\mu) e_i e_i^T$ with entries $f(\phi,\mu) = (\mu_v, \phi\mu_f, \phi\mu_f) \in \mathbb{R}^3_+$ and basis vector $e_i \in \mathbb{R}^n$ with n being the number of dimensions in vector $f(\phi,\mu)$. In this setting, μ_f is fixed to a small value, while we rely on shock detection in the determination of μ_v following Reference 19. We refer to Sections 4.4 and 4.5 for more detailed information.

Remark 2. For classical SWE, a physical interpretation can be obtained for the introduction of the viscous part in the conservation of momentum equation.[20] So far only porous SWE, without additional viscous terms, have been introduced in the literature, hence the usage is justified in Appendix A. Instead of the derived nonlinear formulation, we will work with linear diffusion in the sense of artificial viscosity, that is, for stability also placed on the continuity equation. In this setting, we follow the justification as in Reference 21. We would like to highlight that adjoint-based shape optimization for nonlinear diffusion can be handled in the same way, leading to additional terms in the adjoint equations and the shape derivative.

Remark 3. A constant porosity coefficient $\phi_1 = \phi_2$ in (1) leads to SWE in the classical form, that are subject for adjoint-based shape optimization in Reference 11. A detailed explanation for associated boundary conditions in the inviscid case can be found, for example, in Reference 22.

We finally obtain a PDE-constrained optimization problem by constraining objective

$$J(\Omega) = J_1(\Omega) + J_2(\Omega) + J_3(\Omega) + J_4(\Omega). \tag{18}$$

Here we try to meet certain predefined wave height and velocities $\bar{U}$ at the shore Γ_1 weighted by diagonal matrix $N \in \mathbb{R}^{3\times 3}$, such that we minimize objective $J_1 : \Omega \to \mathbb{R}$, where

$$J_1(\Omega) = \int_0^T \int_{\Gamma_1} \frac{1}{2} \|N(\hat{U}(t,x) - \bar{U}(t,x))\|_2^2 \, \mathrm{d}s \, \mathrm{d}t. \tag{19}$$

This objective is supplemented by a volume penalty, which hinders the obstacle from becoming arbitrarily large

$$J_2(\Omega) = \nu_2 \int_D 1 \, \mathrm{d}x, \tag{20}$$

a perimeter regularization to ensure a sufficient regularity at obstacle level on Γ_3, which lets us define necessary normal vectors, that is,

$$J_3(\Omega) = \nu_3 \int_{\Gamma_3} 1 \, \mathrm{d}s \tag{21}$$

and lastly a thickness control following Reference 23

$$J_4(\Omega) = \nu_4 \int_{\Gamma_3} \int_0^{d_{\min}} \left[\left(d_\Omega \left(x - \xi \vec{n}(x) \right) \right)^+ \right]^2 \mathrm{d}\xi \, \mathrm{d}s. \tag{22}$$

Here d_Ω represents the signed distance function with value

$$d_\Omega(x) = \begin{cases} d(x, \partial\tilde{\Omega}), & \text{if } x \in \tilde{\Omega}, \\ 0, & \text{if } x \in \partial\tilde{\Omega}, \\ -d(x, \partial\tilde{\Omega}), & \text{if } x \in \tilde{\Omega}^c, \end{cases} \tag{23}$$

where the Euclidian distance of $x \in \mathbb{R}^d$ to a closed set $K \subset \mathbb{R}^d$ is defined as

$$d(x, K) = \min_{y \in K} \|x - y\|_2 \tag{24}$$

for Euclidian distance $\|.\|_2$. The three penalty terms are controlled by parameters ν_2, ν_3, and ν_4, which need to be defined a priori (for further details, cf. Section 3).

Remark 4. The first objective (19) is of tracking type[24] to aim for rest-conditions of the water. Regions with comparable properties are known to mitigate sediment transport, for example, as it can be seen in a coupling with equations of Exner-type.[25] Alternatively to (19) the minimization of the mechanical energy of destructive sea-waves may lead to further insights.[6]

3 | DERIVATION OF THE SHAPE DERIVATIVE

We now fix notations and definitions in the first part, before deriving the adjoint equations and shape derivatives in the second part, that are necessary to solve the PDE-constrained optimization problem.

3.1 | Notations and definitions

In this section, we introduce a methodology that is commonly used in shape optimization, extensively elaborated in various works.[1-3] We fix notations and definitions following Reference 4 and amend whenever it appears necessary. We start by introducing a family of mappings $\{\phi_\epsilon\}_{\epsilon \in [0,\tau]}$ for $\tau > 0$ that are used to map each current position $x \in \Omega$ to another by $\phi_\epsilon(x)$, where we choose the vector field $\vec{V}$ as the direction for the so-called perturbation of identity

$$x_\epsilon = \phi_\epsilon(x) = x + \epsilon \vec{V}(x). \tag{25}$$

According to this methodology, we can map the whole domain Ω to another Ω_ϵ such that

$$\Omega_\epsilon = \{x_\epsilon | x + \epsilon \vec{V}(x), x \in \Omega\}. \tag{26}$$

We define the Eulerian derivative as

$$DJ(\Omega)[\vec{V}] = \lim_{\epsilon \to 0^+} \frac{J(\Omega_\epsilon) - J(\Omega)}{\epsilon}. \tag{27}$$

Commonly, this expression is called shape derivative of J at Ω in direction $\vec{V}$ and in this sense J shape differentiable at Ω if for all directions $\vec{V}$ the Eulerian derivative exists and the mapping $\vec{V} \mapsto DJ(\Omega)[\vec{V}]$ is linear and continuous. In addition, we define the material derivative of some scalar function $p : \Omega \to \mathbb{R}$ at $x \in \Omega$ by the derivative of a composed function $p_\epsilon \circ \phi_\epsilon : \Omega \to \Omega_\epsilon \to \mathbb{R}$ for $p_\epsilon : \Omega_\epsilon \to \mathbb{R}$ as

$$D_m p(x) := \lim_{\epsilon \to 0^+} \frac{p_\epsilon \circ \phi_\epsilon(x) - p(x)}{\epsilon} = \frac{d}{d\epsilon} (p_\epsilon \circ \phi_\epsilon)(x)\big|_{\epsilon = 0^+} \tag{28}$$

and the corresponding shape derivative for a scalar p and a vector-valued $\vec{P}$ for which the material derivative is applied component-wise as

$$Dp[\vec{V}] := D_m p - \vec{V} \cdot \nabla p, \tag{29}$$

$$D\vec{P}[\vec{V}] := D_m \vec{P} - \vec{V}^T \nabla \vec{P}. \tag{30}$$

In the following, we will use the abbreviation $\dot{p}$ and $\dot{P}$ to mark the material derivative of p and P. In Section 3, we will make use of the following calculation rules[26]

$$D_m(pq) = D_m pq + pD_m q, \tag{31}$$

$$D_m \nabla p = \nabla D_m p - \nabla \vec{V}^T \nabla p, \tag{32}$$

$$D_m \nabla \vec{P} = \nabla D_m \vec{P} - \nabla \vec{V}^T \nabla \vec{P}, \tag{33}$$

$$D_m(\nabla q^T \nabla p) = \nabla D_m p^T \nabla q - \nabla q^T \left(\nabla \vec{V} + \nabla \vec{V}^T \right) \nabla p + \nabla p^T \nabla D_m q. \tag{34}$$

The basic idea in the derivation of the shape derivative in the next section will be to pull back each integral defined on the on the transformed field back to the original configuration. Hence, we need to state the following rule for differentiating domain integrals[26]

$$\frac{d}{d\epsilon} \left(\int_{\Omega_\epsilon} p_\epsilon \right) \Big|_{\epsilon=0^+} = \int_\Omega (D_m p + \nabla \cdot \vec{V} p). \tag{35}$$

3.2 | Shape derivative

We compute the adjoint equations and the shape derivative of the PDE-constrained optimization problem by formulating the Lagrangian

$$\mathcal{L}(\Omega, U, P) = J_1(\Omega) + a(U, P) - b(P), \tag{36}$$

where J_1 is objective (19), and $a(U,P)$ and $b(P)$ are obtained from boundary value problem (1). Here, we rewrite the equations in weak form by multiplying with some arbitrary test function $P \in H^1(\Omega \times (0,T))^3$ obtaining the form $a(U,P) = a(H, \vec{Q}, p, \vec{r})$, which is defined as

$$\begin{aligned}
a(H, \vec{Q}, p, \vec{r}) := & \int_0^T \int_\Omega \left[\frac{\partial \phi H}{\partial t} + \nabla \cdot (\phi \vec{Q}) \right] p \, \mathrm{d}x \, \mathrm{d}t \\
& + \int_0^T \int_\Omega \mu_v \nabla (H + z) \cdot \nabla p \, \mathrm{d}x \, \mathrm{d}t - \int_0^T \int_{\Gamma_3} [\![\mu_v \nabla (H + z) \cdot \vec{n} p]\!] \, \mathrm{d}s \, \mathrm{d}t \\
& - \int_0^T \int_{\Gamma_2} \mu_v \nabla (H_1 + z) \cdot \vec{n} p \, \mathrm{d}s \, \mathrm{d}t \\
& + \int_0^T \int_\Omega \left[\frac{\partial \phi \vec{Q}}{\partial t} + \nabla \cdot \left(\phi \frac{\vec{Q}}{H} \otimes \vec{Q} + \frac{1}{2} g \phi H^2 \mathbf{I}_2 \right) \right] \cdot \vec{r} \, \mathrm{d}x \, \mathrm{d}t \\
& + \int_0^T \int_\Omega \mu_f \phi \nabla \vec{Q} : \nabla \vec{r} \, \mathrm{d}x \, \mathrm{d}t - \int_0^T \int_{\Gamma_3} [\![\phi \mu_f \nabla \vec{Q} \cdot \vec{n} \cdot \vec{r}]\!] \, \mathrm{d}s \, \mathrm{d}t \\
& + \int_0^T \int_\Omega g \phi H \nabla z \cdot \vec{r} \, \mathrm{d}x \, \mathrm{d}t - \int_0^T \int_\Omega g \frac{H^2}{2} \nabla \phi \cdot \vec{r} \, \mathrm{d}x \, \mathrm{d}t
\end{aligned} \tag{37}$$

and a zero perturbation term.

Remark 5. To deal with well-defined weak forms and to allow us to perform adjoint-based sensitivity analyses, we assume the flow to be free of discontinuities, for example, induced by a discontinuous bottom profile z or wave height H. In addition, we need to employ a specific handle to the discontinuous porosity coefficient. In this article, we have used the strategy to write each integral over Ω as the sum over subdomains $\int_\Omega = \int_{\tilde{\Omega}} + \int_D$. In (37) and in what follows this decomposition is assumed.

Remark 6. For the discontinuous coefficient we could rely on a smoothed porosity controlled by $\alpha > 0$, that is, $\phi = \lim_{\alpha \to 0} \phi_\alpha$, for example, by using smoothed cell transitions or mollifiers. In this setting, we could integrate over the whole domain Ω. Such a handle would call for the necessity to show convergence results for state, adjoint and shape derivative.

Furthermore, we remark that a smoothing approach is presented in one dimension in Appendix E, where we have used a smoothed step-function. Here interface conditions would not be required in the continuous form.

We obtain state equations from differentiating the Lagrangian w.r.t. P and the auxiliary problem, the adjoint equations, from differentiating the Lagrangian w.r.t. the states U. The adjoint is formulated in the following theorem:

Theorem 1 (Adjoint). *Assume that the parabolic PDE problem (1) is H^1-regular, so that its solution U is at least in $H^1(\Omega \times (0,T))^3$. Then the adjoint in strong form with solution $P = (p, \vec{r}) \in H^1(\Omega \times (0,T))^3$ is given by*

$$\phi\left[-\frac{\partial p}{\partial t} + \frac{1}{H^2}(\vec{Q}\cdot\nabla)\vec{r}\cdot\vec{Q} - gH(\nabla\cdot\vec{r}) + g\nabla z\cdot\vec{r}\right] \; - \nabla\cdot(\mu_v\nabla p) - gH\nabla\phi\cdot\vec{r} = -N_{11}((H+z)-\overline{H})_{\Gamma_1} \tag{38}$$

and

$$\phi\left[-\frac{\partial \vec{r}}{\partial t} - \nabla p - \frac{1}{H}(\vec{Q}\cdot\nabla)\vec{r} - \frac{1}{H}(\nabla\vec{r})^T\vec{Q}\right] \; - \nabla\cdot(\mu_f\phi\nabla\vec{r}) = -G(N_{22,33})(\vec{Q}-\bar{\vec{Q}})_{\Gamma_1} \tag{39}$$

with outer boundaries

$$\begin{aligned}
&p = 0, && \text{in } \Omega\times\{T\},\\
&\vec{r} = 0, && \text{in } \Omega\times\{T\},\\
&\vec{r}\cdot\vec{n} = 0,\ \nabla p\cdot\vec{n} = 0,\ \nabla r_1\cdot\vec{n} = 0,\ \nabla r_2\cdot\vec{n} = 0, && \text{on } \Gamma_1\times(0,T),\\
&\phi p\vec{n} + \frac{\phi}{H_1}(\vec{Q}\cdot\vec{n})\vec{r} + \frac{\phi}{H_1}(\vec{Q}\vec{r})\cdot\vec{n} = 0,\ \nabla r_1\cdot\vec{n} = 0,\ \nabla r_2\cdot\vec{n} = 0, && \text{on } \Gamma_2\times(0,T)
\end{aligned} \tag{40}$$

and interface boundaries on Γ_3 as

$$[\![p]\!] = 0, \tag{41}$$

$$[\![\vec{r}]\!] = 0 \tag{42}$$

such as

$$[\![\nabla p\cdot\vec{n}]\!] = 0, \tag{43}$$

$$[\![\phi\nabla r_1\cdot\vec{n}]\!] = 0, \tag{44}$$

$$[\![\phi\nabla r_2\cdot\vec{n}]\!] = 0 \tag{45}$$

and

$$[\![\phi F_U(P)\cdot\vec{n}]\!] = 0, \tag{46}$$

that is,

$$\left[\!\!\left[\phi\left(\frac{\vec{Q}}{H^2}\cdot\vec{r}\vec{Q} + gH\vec{r}\right)\cdot\vec{n}\right]\!\!\right] = 0, \tag{47}$$

$$[\![\phi(p + 2Q_1/Hr_1 + Q_2/Hr_2; Q_2/Hr_1)\cdot\vec{n}]\!] = 0, \tag{48}$$

$$[\![\phi(Q_1/Hr_1; p + 2Q_2/Hr_2 + Q_1/Hr_2)\cdot\vec{n}]\!] = 0. \tag{49}$$

Proof. See Appendix B. ∎

The porous SWE adjoint can be written in vector form as

$$-\phi\frac{\partial P}{\partial t} + \phi AP_x + \phi BP_y + \phi CP - \nabla\cdot(G(f(\phi,\mu))\nabla P) = S, \tag{50}$$

where

$$A = \begin{pmatrix} 0 & \frac{Q_1}{H^2} - gH & \frac{Q_1 Q_2}{H^2} \\ -1 & -2\frac{Q_1}{H} & -\frac{Q_2}{H} \\ 0 & 0 & -\frac{Q_1}{H} \end{pmatrix}, \quad B = \begin{pmatrix} 0 & \frac{Q_1 Q_2}{H^2} & \frac{Q_2^2}{H^2} - gH \\ 0 & -\frac{Q_2}{H} & 0 \\ -1 & -\frac{Q_1}{H} & -2\frac{Q_2}{H} \end{pmatrix}, \tag{51}$$

and C originates from variations in the sediment and the porosity such that

$$C = \begin{pmatrix} 0 & g\frac{\partial z}{\partial x} - g\frac{H}{\phi}\frac{\partial \phi}{\partial x} & g\frac{\partial z}{\partial y} - g\frac{H}{\phi}\frac{\partial \phi}{\partial y} \\ 0 & 0 & 0 \\ 0 & 0 & 0 \end{pmatrix}. \tag{52}$$

Remark 7. In this article, we will only consider the volume form of the shape derivative, which will be used to obtain smooth mesh deformations by a Riesz projection.

Theorem 2 (Shape derivative). *Assume that the parabolic PDE problem (1) is H^1-regular, so that its solution U is at least in $H^1(\Omega \times (0,T))^3$. Moreover, assume that the adjoint equations (50) admit a solution $P \in H^1(\Omega \times (0,T))^3$. Then the shape derivative of the objective J_1 at Ω in the direction $\vec{V}$ is given by*

$$\begin{aligned} DJ_1(\Omega)[\vec{V}] = \int_0^T \int_\Omega \Bigg[& -(\nabla \vec{V})^T : \nabla(\phi \vec{Q}) p - (\nabla \vec{V})^T : \nabla \vec{Q} \frac{\phi \vec{Q}}{H} \cdot \vec{r} \\ & - (\nabla \vec{V} \vec{Q} \cdot \nabla) \frac{\phi \vec{Q}}{H} \cdot \vec{r} - gH(\nabla \vec{V})^T \nabla(\phi H) \cdot \vec{r} \\ & - \mu_v \nabla(H+z)^T (\nabla \vec{V} + \nabla \vec{V}^T) \nabla p \\ & - \phi \mu_f \nabla \vec{Q} \nabla \vec{V} : \nabla \vec{r} - \phi \mu_f \nabla \vec{Q} \nabla \vec{V}^T : \nabla \vec{r} \\ & - g\phi H \nabla \vec{V}^T \nabla z \cdot \vec{r} + \frac{1}{2} g H^2 \nabla \vec{V}^T \nabla \phi \cdot \vec{r} \\ \times + & \operatorname{div}(\vec{V}) \left\{ \frac{\partial \phi H}{\partial t} p + \nabla \cdot (\phi \vec{Q}) p + \frac{\partial \phi \vec{Q}}{\partial t} \cdot \vec{r} \right. \\ & + \phi(\vec{Q} \cdot \nabla) \frac{\vec{Q}}{H} \cdot \vec{r} + \nabla \cdot (\phi \vec{Q}) \frac{\vec{Q}}{H} \cdot \vec{r} + \frac{1}{2} g \nabla(\phi H^2) \cdot \vec{r} \\ & + g\phi H \nabla z \cdot \vec{r} + \mu_v \nabla(H+z) \cdot \nabla p \\ & \left. + \ \phi \mu_f \nabla \vec{Q} : \nabla \vec{r} - g \frac{1}{2} H^2 \nabla \phi \cdot \vec{r} \right\} \Bigg] \ \mathrm{d}x \, \mathrm{d}t. \end{aligned} \tag{53}$$

Proof. See Appendix C. ∎

The shape derivatives of the penalty terms (volume, perimeter and thickness) are obtained as, see, for example, Reference 2

$$DJ_2(\Omega)[\vec{V}] = \nu_2 \int_D \nabla \cdot \vec{V} \, \mathrm{d}x, \tag{54}$$

$$DJ_3(\Omega)[\vec{V}] = \nu_3 \int_{\Gamma_3} \kappa \langle \vec{V}, \vec{n} \rangle \, \mathrm{d}s, \tag{55}$$

and see Reference 23 for

$$\begin{aligned} DJ_4(\Omega)[\vec{V}] = \nu_4 \int_{\Gamma_3} \int_0^{d_{\min}} \Big[& \vec{V}(x) \cdot \vec{n}(x) \left\{ \kappa(x) (d_\Omega(x_m)^+)^2 \right. \\ & \left. + \ 2 d_\Omega(x_m)^+ \nabla d_\Omega(x_m) \cdot \nabla d_\Omega(x) \right\} \\ & - \vec{V}(p_{\partial\Omega}(x_m)) \cdot \vec{n}(p_{\partial\Omega}(x_m)) 2 (d_\Omega(x_m))^+ \Big] \ \mathrm{d}\xi \, \mathrm{d}s \end{aligned} \tag{56}$$

for mean curvature κ and offset point $x_m = x - \xi\vec{n}(x)$, where we require the shape derivative of the signed distance function[3]

$$Dd_\Omega(x)[\vec{V}] = -\vec{V}(p_{\partial\Omega}(x)) \cdot \vec{n}(p_{\partial\Omega}(x)) \tag{57}$$

with operator $p_{\partial\Omega}$ that projects a point $x \in \Omega$ onto its closest boundary and holds for all $x \notin \Sigma$, where Σ is referred to as the ridge, where the minimum in (24) is obtained by two distinct points.

4 | NUMERICAL RESULTS

In the first part of this section, we shortly sketch the SIP-DG method as in Reference 17, before we discuss the well-balancedness of the porous SWE with diffusive terms and describing the algorithm for shape optimization in detail. Results are finally tested in two different scenarios.

4.1 | SIP-DG

As in Reference 11, we solve the boundary value problem (1), the adjoint problem (50) such as all quantities of the objective (18) with the finite element solver FEniCS.[27] For the time discretization, we can choose between implicit and explicit integration arising from theta-methods.[28] High accuracy even for the inviscid and hyperbolic PDE is achieved using a SIP-DG method to discretize in space.[17] This implies discontinuous cell transitions, and hence a formulation based on each element $\kappa \in \mathcal{T}_h$ or facet Γ_I for a subdivision $\mathcal{T}_h$ of some domain Ω, such as a redefinition of each function and operator on the so-called broken and possibly vector-valued d-dimensional Sobolov space $\mathcal{H}^m(\mathcal{T}_h \times (0,T))^d$. In this light, we also need to define the average $\{\{U\}\} = (U^+ + U^-)/2$ and jump term $\underline{[\![U]\!]} = U^+ \otimes n_+ + U^- \otimes n_-$ to express fluxes on cell transitions. The discretization then reads for solution and test-function $U_h, P_h \in \mathcal{H}^1(\mathcal{T}_h \times (0,T))^3$ as[17,29]

$$\begin{aligned}
N_h(U_h, P_h) = &\int_0^T \int_\Omega \left[\frac{\partial \phi_h U_h}{\partial t} \cdot P_h - \phi_h F(U_h) : \nabla_h P_h + G(f(\phi_h, \mu))\nabla_h(\hat{U}_h) : \nabla_h P_h \right. \\
&\left. - \phi_h S(U_h) \cdot P_h - S_\phi(U_h) \cdot P_h \right] \mathrm{d}x \, \mathrm{d}t \\
&+ \int_0^T \sum_{\kappa \in \mathcal{T}_h} \int_{\partial\kappa \setminus \Gamma} \mathcal{F}(U_h^+, U_h^-, \vec{n}^+) \cdot P_h^+ \, \mathrm{d}s \, \mathrm{d}t \\
&+ \int_0^T \int_{\Gamma_I} \left[\underline{\delta_h} : \underline{[\![P_h]\!]} \, \mathrm{d}s \, \mathrm{d}t - \{\{G(f(\phi_h, \mu))\nabla_h(P_h)\}\} : \underline{[\![\hat{U}_h]\!]} \right. \\
&\left. - \{\{G(f(\phi_h, \mu))\nabla_h(\hat{U}_h)\}\} : \underline{[\![P_h]\!]} \right] \mathrm{d}s \, \mathrm{d}t + N_{\Gamma,h}(U_h, P_h, \phi_h),
\end{aligned} \tag{58}$$

where fluxes at the discontinuous cell transitions are defined by the numerical flux function $\mathcal{F}(U_h^{+,*}, U_h^{-,*}, \vec{n}^+)$.

Remark 8. For the advective flux and for a given flux Jacobian $J_i := \partial_U F_i(U)$ and matrix $B(U, \vec{n}) = \sum_{i=1}^2 n_i J_i(U)$, we can choose between a variety of fluxes.[30] From here on the (local) Lax–Friedrichs flux is used that is defined as

$$\mathcal{F}(U^+, U^-, \vec{n})|\partial\kappa = \frac{1}{2}\left(F(U^+) \cdot \vec{n} + F(U^-) \cdot \vec{n} + \alpha_{\max}(U^+ - U^-)\right), \tag{59}$$

where $\alpha_{\max} = \max_{V=U^+,U^-}\{|\lambda(B(V, \vec{n}_\kappa))|\}$ with $\lambda(B(V, \vec{n}_\kappa))$ returning a sequence of eigenvalues for the matrix B restricted on a side of element κ.

Remark 9. For the classical SWE, eigenvalues of the SWE-Jacobian are obtained following Reference 30, where $c = \sqrt{gH}$ denotes the wave celerity, as

$$\begin{aligned}
\lambda(n_1 J_1 + n_2 J_2) &= \{\lambda_1, \lambda_2, \lambda_3\} \\
&= \{un_1 + vn_2 - c, un_1 + vn_2, un_1 + vn_2 + c\}.
\end{aligned} \tag{60}$$

Remark 10. We would like to highlight, that the chosen interface condition, can be resolved in an SIP-DG scheme for cells at the interface as well. Hence, the summation of all integrals of interior cell boundaries $\sum_{\kappa\in\mathcal{T}_h}\int_{\partial\kappa\setminus\Gamma}$ in (58) includes the interface boundary Γ_3. We show this in Appendix D.

In (58), we define the penalization term for the viscous fluxes as[17]

$$\underline{\delta}_h(\hat{U}_h) = C_{\mathrm{IP}}\frac{p_{\mathrm{DG}}^2}{h_\kappa}\{\{G(f(\phi_h^+,\mu))\}\}\underline{[\![\hat{U}_h]\!]}, \tag{61}$$

where $C_{\mathrm{IP}} > 0$ is a constant, $p_{\mathrm{DG}} > 0$ the polynomial order of the DG method and $h_\kappa > 0$ the element-diameter for $\kappa \in \mathcal{T}_h$. What is remaining in (58) is the specification of the boundary term, here we state that

$$\begin{aligned} N_{\Gamma,h}(U_h,P_h) = &\int_0^T\int_\Gamma \mathcal{F}(U_h^+,U_\Gamma(U_h^+),\vec{n})\cdot P_h^+ \,\mathrm{d}s\,\mathrm{d}t \\ &+\int_0^T\int_{\Gamma_n}\Big[\underline{\delta}_\Gamma(U_h^+) : P_h^+\otimes\vec{n}^+ + G(f(\phi_h^+,\mu))\nabla_h(\hat{U}_h^+) : P_h^+\otimes\vec{n} \\ &- G(f(\phi_h^+,\mu))\nabla_h V_h^+ : (\hat{U}_h^+ - U_\Gamma(\hat{U}_h^+))\otimes\vec{n}\Big]\,\mathrm{d}s\,\mathrm{d}t, \end{aligned} \tag{62}$$

where Γ_n are all boundaries of type Neumann. Additionally, we define

$$\underline{\delta}_\Gamma(U_h^+) = C_{\mathrm{IP}}G(f(\phi_h^+,\mu))\frac{p_{\mathrm{DG}}^2}{h_\kappa}(U_h^+ - U_\Gamma(U_h^+))\otimes\vec{n}, \tag{63}$$

$$\mathcal{F}(U_h^+,U_\Gamma(U_h^+),\vec{n}^+) = \frac{1}{2}[\vec{n}^+\cdot F(U_h^+) + \vec{n}^+\cdot F(U_\Gamma(U_h^+))]. \tag{64}$$

For the pure advective SWE, open and rigid-wall boundary functions are defined as in Reference 30.

4.2 | Well-balancedness of SIP-DG for porous SWE

Approximate numerical solutions to systems like (1), which allow to properly handle shocks and contact discontinuities, are in general known to be inaccurate even for near steady states.[31] This difficulty can be overcome by using the so-called well-balanced schemes, first introduced in Reference 32. We will derive this property for our numerical scheme for the case of one-dimensional equations extending the approach in Reference 18 to porous SWE with diffusive terms. The two-dimensional formulation follows immediately then. Before starting, we explicitly state that we rely our solver on variables

$$\tilde{U} = \begin{pmatrix} h \\ uh \end{pmatrix} = \begin{pmatrix} \phi H \\ \phi u H \end{pmatrix}. \tag{65}$$

Hence, we redefine the 1D porous SWE without diffusion in vector notation as

$$\partial_t(\tilde{U}) + \nabla\cdot(F(\tilde{U})) = S(\tilde{U}) + S_\phi(\tilde{U}) \tag{66}$$

for given flux matrix

$$F(\tilde{U}) = \begin{pmatrix} hu \\ hu^2 + \frac{1}{2}gh^2/\phi \end{pmatrix} \tag{67}$$

and as before a source regarding the variations in the sediment

$$S(\tilde{U}) = \begin{pmatrix} 0 \\ -gh\frac{\partial z}{\partial x} \end{pmatrix} \tag{68}$$

and variations in the porosity factor

$$S_\phi(\tilde{U}) = \begin{pmatrix} 0 \\ \frac{g}{2}\frac{h^2}{\phi^2}\frac{\partial \phi}{\partial x} \end{pmatrix}. \tag{69}$$

Well-balancing relies on incorporating the discretization of the source term in fluxes, such that, for example, (59) used in (58) is redefined. Preserving still water stationary conditions means that $uh = 0$ for $h/\phi + z = C$ for all $t \in (0, T)$. For the contribution to time changes, it should be justified that on each element $\kappa \in \mathcal{T}_h = [x_{j-1/2}, x_{j+1/2}]$

$$\begin{aligned} R = &- \int_\kappa F(\tilde{U}_h(x,t)) \cdot \partial_x P_h(x)\, \mathrm{d}x + \mathcal{F}^L_{j+1/2} \cdot P_h\left(x^-_{j+1/2}\right) - \mathcal{F}^R_{j-1/2} \cdot P_h\left(x^+_{j-1/2}\right) \\ &- \int_\kappa S(\tilde{U}_h(x,t)) \cdot P_h(x)\, \mathrm{d}x - \int_\kappa S_\phi(\tilde{U}_h(x,t)) \cdot P_h(x)\, \mathrm{d}x = 0. \end{aligned} \tag{70}$$

In Reference 18, it is stated that Equation (70) is fulfilled if,

1. $\mathcal{F}^L_{j+1/2} = F(\tilde{U}_h(x^-_{j+1/2}))$ and $\mathcal{F}^R_{j-1/2} = F(\tilde{U}_h(x^+_{j-1/2}))$.
2. We are in a steady state and u_h is a numerical approximation of u, hence

$$\partial_x F(\tilde{U}_h) = \begin{pmatrix} 0 \\ g(h_h, z_h, \phi_h) \end{pmatrix}.$$

The assumption above can be easily justified and shows the appropriateness of the unmodified scheme in case of continuous piecewise sediment $z_h(x^-_{j+1/2}) = z_h(x^+_{j+1/2})$ and porosity coefficients $\phi_h(x^-_{j+1/2}) = \phi_h(x^+_{j+1/2})$. Situations with discontinuous sediment are dealt by relying on the idea of redefining variables,[33] that is,

$$h^{+,*}_{h,j+1/2} = \max\left(0, h^+_{h,j+1/2} + z^+_{h,j+1/2} - \max\left(z^+_{h,j+1/2}, z^-_{h,j+1/2}\right)\right), \tag{71}$$

$$h^{-,*}_{h,j+1/2} = \max\left(0, h^-_{h,j+1/2} + z^-_{h,j+1/2} - \max\left(z^+_{h,j+1/2}, z^-_{h,j+1/2}\right)\right), \tag{72}$$

which can be extended for varying porosity coefficient to

$$h^{+,*}_{h,j+1/2} = \max\left(0, \frac{h^+_{h,j+1/2}}{\phi^+_{h,j+1/2}} + z^+_{h,j+1/2} - \max\left(z^+_{h,j+1/2}, z^-_{h,j+1/2}\right)\right) \min\left(\phi^+_{h,j+1/2}, \phi^-_{h,j+1/2}\right), \tag{73}$$

$$h^{-,*}_{h,j+1/2} = \max\left(0, \frac{h^-_{h,j+1/2}}{\phi^-_{h,j+1/2}} + z^-_{h,j+1/2} - \max\left(z^+_{h,j+1/2}, z^-_{h,j+1/2}\right)\right) \min\left(\phi^+_{h,j+1/2}, \phi^-_{h,j+1/2}\right) \tag{74}$$

such that

$$\tilde{U}^{+,*}_{h,j+1/2} = \begin{pmatrix} h^{+,*}_{h,j+1/2} \\ uh^+_{h,j+1/2} \end{pmatrix}. \tag{75}$$

Theorem 3 (Well-balancedness). *Redefining $\tilde{U}^{\pm,*}_{h,j+1/2}$ as in (75) in accordance with corrector-terms lead to a well-balanced scheme*

Proof.

$$\begin{aligned} \mathcal{F}^L_{j+1/2} &= \mathcal{F}\left(\tilde{U}^{-,*}_{h,j+1/2}, \tilde{U}^{+,*}_{h,j+1/2}\right) \\ &\quad + \begin{pmatrix} 0 \\ \frac{g}{2}\left(h^-_{h,j+1/2}\right)^2/\phi^-_{h,j+1/2} - \frac{g}{2}\left(h^{-,*}_{h,j+1/2}\right)^2/\min\left(\phi^+_{h,j+1/2}, \phi^-_{h,j+1/2}\right) \end{pmatrix} \\ &= F(\tilde{U}^-_{h,j+1/2}). \end{aligned}$$

Similarly

$$\mathcal{F}^R_{j-1/2} = F\left(\tilde{U}^+_{h,j-1/2}\right).$$

■

Extending results to two dimensions can be done by looking at the residual on an element $\kappa \in \mathcal{T}_h$

$$\begin{aligned} R = &-\int_\kappa F(\tilde{U}_h(x,t)) : \nabla P_h(x)\, \mathrm{d}x + \int_{\partial\kappa} \mathcal{F}_{\partial\kappa}(U^+_h(x,t), U^-_h(x,t), \vec{n}^+) \cdot P^+_h \, \mathrm{d}s \\ &- \int_\kappa S(\tilde{U}_h(x,t)) \cdot P_h(x)\, \mathrm{d}x - \int_\kappa S_\phi(\tilde{U}_h(x,t)) \cdot P_h(x)\, \mathrm{d}x = 0 \end{aligned} \tag{76}$$

and relying on a flux modification on each elemental boundary as

$$\mathcal{F}_{\partial\kappa} = \mathcal{F}\left(\tilde{U}^{-,*}_{h,\partial\kappa}, \tilde{U}^{+,*}_{h,\partial\kappa}, \vec{n}^+_{\partial\kappa}\right) \tag{77}$$

$$+ G\begin{pmatrix} 0 \\ \vec{n}^+_{0,\partial\kappa} \\ \vec{n}^+_{1,\partial\kappa} \end{pmatrix}\begin{pmatrix} 0 \\ \frac{g}{2}\left(h^+_{h,\partial\kappa}\right)^2/\phi^+_{h,\partial\kappa} - \frac{g}{2}\left(h^{+,*}_{h,\partial\kappa}\right)^2/\min\left(\phi^+_{h,\partial\kappa}, \phi^-_{h,\partial\kappa}\right) \\ \frac{g}{2}\left(h^+_{h,\partial\kappa}\right)^2/\phi^+_{h,\partial\kappa} - \frac{g}{2}\left(h^{+,*}_{h,\partial\kappa}\right)^2/\min\left(\phi^+_{h,\partial\kappa}, \phi^-_{h,\partial\kappa}\right) \end{pmatrix}, \tag{78}$$

where

$$\tilde{U}^{+,*}_{h,\partial\kappa} = \begin{pmatrix} h^{+,*}_{h,\partial\kappa} \\ uh^+_{h,\partial\kappa} \\ vh^+_{h,\partial\kappa} \end{pmatrix}. \tag{79}$$

Remark 11. Adding diffusive terms in the form

$$\partial_t(\tilde{U}) + \nabla\cdot(F(\tilde{U})) - \nabla\cdot(G(f(\phi,\mu))\nabla\hat{U}) = S(\tilde{U}) + S_\phi(\tilde{U}),$$

where $\hat{U} = (z + h/\phi, uh, vh)$, does not disturb well-balancedness, since rest conditions cancel contributing terms.

Remark 12. Reformulation (65) requires eigenvalues in the form of (60) with $c = \sqrt{gh/\phi}$ to be used in the numerical flux function.

Remark 13. The numerical scheme used to handle discontinuous sediment and porosity coefficients forms the limit of a smoothed scenario, such that $U_\alpha \to U$ in $H^1(\Omega\times(0,T))^3$ where $\phi_\alpha \to \phi$ for $\alpha \to 0$ which is verified for one dimension numerically in Appendix E.

4.3 | Implementation details for shape optimization

We rely on the classical structure of adjoint and gradient-descent based shape optimization algorithms shortly sketched in Algorithm 1.

Algorithm 1. Shape optimization algorithm

Initialization
while $\|DJ(\Omega_k)[\vec{V}]\| > \epsilon_{TOL}$ **do**
1. Calculate SDF w_k
2. Calculate State U_k via $\tilde{U}_k$
3. Calculate Adjoint P_k via $\tilde{P}_k$
4. Use $DJ_{1,2,3,4}(\Omega_k)[\vec{V}]$ to calculate Gradient W_k
5. Perform Linesearch for $\tilde{W}_k$
6. Deform $\Omega_{k+1} \longleftarrow \phi_{\tilde{W}_k}(\Omega_k)$

end while

The signed distance function in (22) is calculated as the solution to the Eikonal equation with $f(x) = 1$, $q(x) = 0$

$$\begin{aligned} |\nabla w(x)| &= f(x), \quad x \in \Omega, \\ w(x) &= q(x), \quad x \in \partial\tilde{\Omega}, \end{aligned} \tag{80}$$

where we solve a stabilized viscous version to obtain $w \in H^1(\Omega)$ for all $v \in H^1(\Omega)$, that is,

$$\int_\Omega \sqrt{\nabla w \cdot \nabla w} v \, \mathrm{d}x - \int_\Omega f v \, \mathrm{d}x + \int_\Omega \mu_{\mathrm{SDF}} \nabla w \cdot \nabla v \, \mathrm{d}x = 0, \tag{81}$$

where $\mu_{\mathrm{SDF}} = \max h_\kappa$ is dependent on the element-diameter h_κ. Numerical solutions to the adjoint equations require us to rewrite the vector form (50) with the help of the product rule, that is,

$$\frac{\partial P}{\partial t} - \nabla \cdot (AP, BP) - \tilde{C}P + \nabla \cdot (G(f(\phi, \mu))\nabla P) = -S, \tag{82}$$

where $\tilde{C}$ is defined to be

$$\tilde{C} = C - A_x - B_y. \tag{83}$$

As we have shown in Reference 11, the eigenvalues of matrix $B^*(P, \vec{n})$ belonging to the adjoint flux Jacobian $\mathcal{J}_i^* := \partial_P F_i^*(P)$ equal the eigenvalues of matrix $B(U, \vec{n})$ belonging to the flux Jacobian $\mathcal{J}_i := \partial_U F_i(U)$. The SWE adjoint problem is then solved in the same manner as the scheme for the forward system (4.1) with (4.2), using a well-balanced SIP-DG discretization in space and a member of the theta-methods for the time discretization.

The finite element mesh $\mathcal{T}_h$ deforms in each iteration via the solution $\vec{W} : \Omega \to \mathbb{R}^2$ of the linear elasticity equation[4]

$$\begin{aligned} \int_\Omega \sigma(\vec{W}) : \epsilon(\vec{V}) \, \mathrm{d}x &= DJ(\Omega)[\vec{V}], \qquad \forall \vec{V} \in H_0^1(\Omega, \mathbb{R}^2), \\ \sigma &:= \lambda_{\mathrm{elas}} \mathrm{Tr}(\epsilon(\vec{W}))I + 2\mu_{\mathrm{elas}}\epsilon(\vec{W}), \\ \epsilon(\vec{W}) &:= \frac{1}{2}\left(\nabla \vec{W} + \nabla \vec{W}^T\right), \\ \epsilon(\vec{V}) &:= \frac{1}{2}\left(\nabla \vec{V} + \nabla \vec{V}^T\right), \end{aligned} \tag{84}$$

where σ and ϵ are called strain and stress tensor and λ_{elas} and μ_{elas} are called Lamé parameters. We have chosen $\lambda_{\mathrm{elas}} = 0$ and μ_{elas} as the solution of the following Poisson Problem

$$\begin{aligned} -\triangle \mu &= 0, \qquad \text{in } \Omega, \\ \mu &= \mu_{\max}, \quad \text{on } \Gamma_3, \\ \mu &= \mu_{\min}, \quad \text{on } \Gamma_1, \Gamma_2. \end{aligned} \tag{85}$$

The source term $DJ(\Omega)[\vec{V}]$ in (84) consists of a volume and surface part, that is, $DJ(\Omega)[\vec{V}] = DJ_\Omega[\vec{V}] + DJ_{\Gamma_3}[\vec{V}]$.

Remark 14. The volumetric share comes from our porous SWE shape derivative and the volume penalty. Before assembling, the test vector fields whose support does not intersect with the interface Γ_3 are set to zero.[4] The surface part comes from the parameter regularization and the thickness constraint in (18).

Remark 15. To guarantee the attainment of useful shapes, which minimize the objective, a backtracking line search is used, which limits the step size in case the shape space is left,[4] that is, having intersecting line segments or in the case of a nondecreasing objective evaluation. As described in Algorithm 1, the iteration is finally stopped if the norm of the shape derivative has become sufficiently small.

4.4 | Example: The half-circled mesh

In the first example, we will look at the model problem—the half circle that was described in Section 2. As before, we interpret $\Gamma_1, \Gamma_2, \Gamma_3$ as coastline, open sea, and obstacle boundary. We will work with a rest height of the water at $\overline{H} = 1$, while

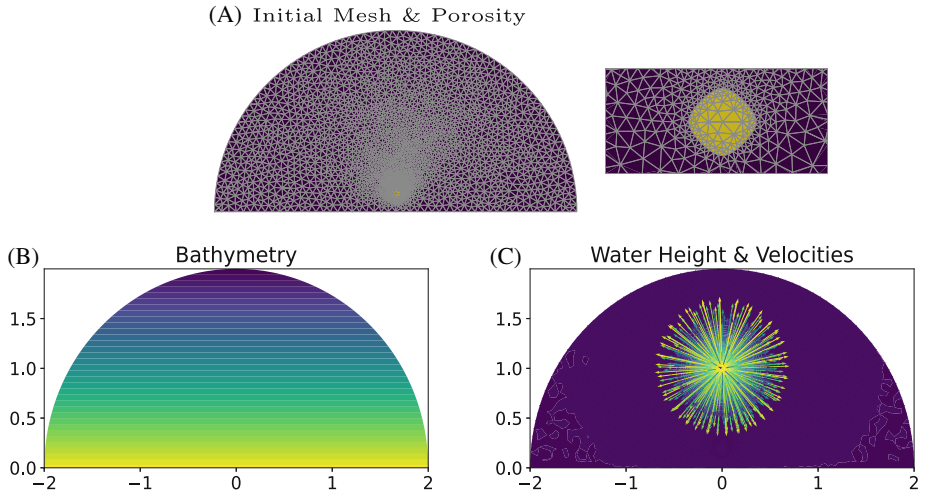

FIGURE 3 (A) Initial mesh and porosity with enlarged image section, (B) linear bathymetry, and (C) field state at $t = 0.1$

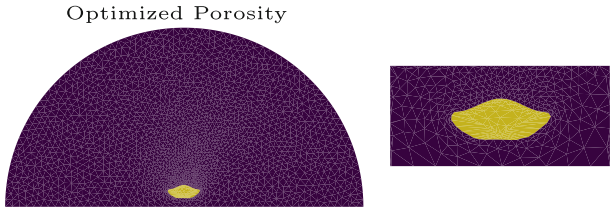

FIGURE 4 Optimized porous region with enlarged image section

targeting zeroed velocities. We penalize volume and thinness by setting $\nu_2 = 1e-4$, $\nu_4 = 1e-2$ and enforce a stronger regularization by $\nu_3 = 1e-4$. The parameters in the porous shallow water system are set as follows: For the weight of the diffusion terms in the momentum equation, we set $\mu_f = 1e-2$ and determine μ_v by the usage of the mentioned shock detector.[19] The gravitational acceleration is fixed at roughly 9.81. The mesh $\mathcal{T}_h$ displayed in Figure 3 was created using the finite element mesh generator GMSH,[34] where the vertex density around the obstacle is increased to ensure a high resolution.

The material coefficient is at $\phi_2 = 0.4$ at D and we obtain classical SWE on $\tilde{\Omega}$ by setting $\phi_1 = 1$. In addition, we employ Gaussian initial conditions as $(H_0 + z, uH_0, vH_0) = (1 + \exp(-15x^2 - 15(y-1)^2), 0, 0)$, which result into a wave traveling in time toward the boundaries. We prescribe the boundary conditions as before, using rigid-wall and outflow boundary conditions for Γ_1 and Γ_2. In this example, we have used a backward Euler time-scheme, that arises from the theta-method for $\theta = 1$, such as a SIP-DG-method of first order that was described before in Section 4.1. For the spatial discretization, we have used $C_{\mathrm{IP}} = 20$ in the SIP-DG method. Solving the state equations requires the definition of the time-horizon $T = 2$, which is chosen to include the travel of a wave to and from the shore using a time-stepping size of $\mathrm{d}t = 2e-3$. Our calculations are performed for a linear decreasing time-constant sediment $z = 0.5 - 0.25y$. Having solved state and adjoint equations the mesh deformation is performed for initial step size $\rho = 1.5$ as described in Section 4.3, where we specify $\mu_{\min} = 10$ and $\mu_{\max} = 100$ in (85). In Figure 4, the result of the shape optimization procedure is displayed after 24 iterations, where deformations appear to be symmetric. As we observe in Figure 5, we have achieved a notable decrease in the objective functional.

4.5 | Example: The Mentawai islands

The second example will investigate an archipelago in the southwest of Sumatra, Indonesia the Mentawai islands, which have turned out to be an effective shield in the 2004 and 2010 tsunami for the mainland located behind.[35] Mentawai islands are threatened by rising sea levels and victim to massive floodings in the last decades and are hence offering itself

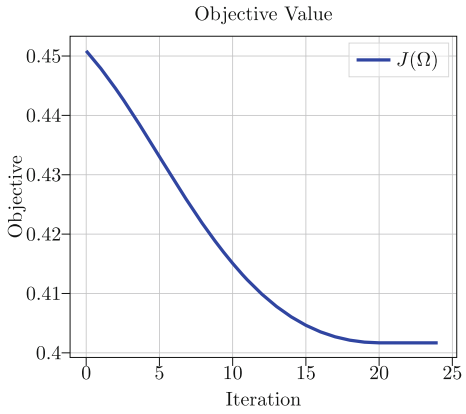

FIGURE 5 Objective value per iteration

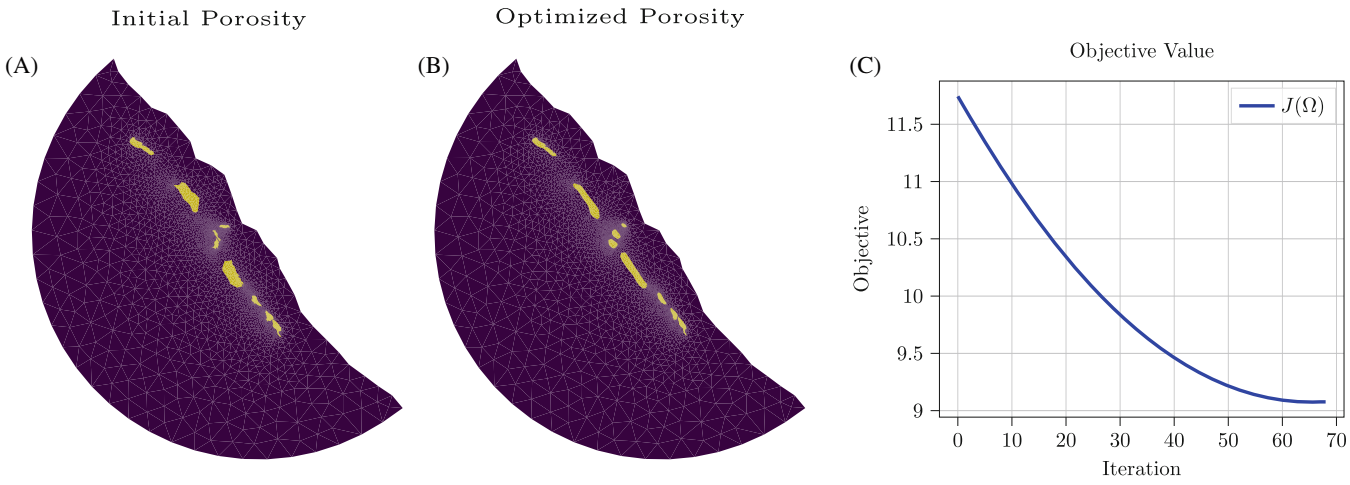

FIGURE 6 (A) Initial porosity, (B) optimized porosity, and (C) objective value per iteration

for protective measures. Real coastal applications require suitable mesh representations. Shorelines are taken from the GSHHG* databank, where we use a geographical information system QGIS3 to process the data to GMSH for the mesh generation.[36] For computational ease, we have decided to not consider smaller islands of a diameter less than 5 km. Similar to the preceding example, we interpret Γ_1 as coastline of the mainland, Γ_2 as the open sea boundary such as Γ_3 as the interface boundary of the offshore islands. Assuming that islands are flooded, we represent them by a difference in the material coefficient, which shape is to be optimized. For this we set $\phi_2 = 0.5$ at D and $\phi_1 = 1$ on $\tilde{\Omega}$ (cf. Figure 6A). As before, we are in a tsunami-like setting and start with suitable Gaussian initial conditions for the height of the water. For simplicity, the sediment height is assumed to be zero on the whole domain. The remaining model-settings are similar to Section 4.4. We can once more observe convergence in the objective, after applying shape optimization on the porous region (cf. Figure 6B,C). The obstacles are enlarged in perpendicular direction to the incoming sea wave.

5 | CONCLUSION

We have investigated porous SWE, where the difference in the material coefficient can be interpreted as a permeable obstacle, that is placed in before shores. We have derived a well-balanced SIP-DG scheme to solve for the evolution of the waves. Based on this solution we have derived the time-dependent continuous adjoint and shape derivative in volume

*https://www.ngdc.noaa.gov/mgg/shorelines/ (last visited May 5, 2022).

form. Results were tested successfully in two scenarios, where the obstacle's shape has been optimized to target a rest height at the shore. Results can be easily adjusted for arbitrary meshes, objective functions and different wave properties driven by initial and boundary conditions as partially shown in Reference 11.

ACKNOWLEDGMENTS

This work has been supported by the Deutsche Forschungsgemeinschaft within the Priority program SPP 1962 "Non-smooth and Complementarity-based Distributed Parameter Systems: Simulation and Hierarchical Optimization." The authors would like to thank Diaraf Seck (Université Cheikh Anta Diop, Dakar, Senegal) and Mame Gor Ngom (Université Cheikh Anta Diop, Dakar, Senegal) for helpful and interesting discussions within the project Shape Optimization Mitigating Coastal Erosion (SOMICE). Open Access funding enabled and organized by Projekt DEAL.

ORCID

Luka Schlegel https://orcid.org/0000-0001-9930-065X
Volker Schulz https://orcid.org/0000-0001-7665-130X

REFERENCES

1. Choi KK. Shape design sensitivity analysis and optimal design of structural systems. In: Mota Soares CA, ed. *Computer Aided Optimal Design: Structural and Mechanical Systems*. Springer; 1987:439-492.
2. Sokołowski J, Zolésio J. *Introduction to Shape Optimization: Shape Sensitivity Analysis*. Springer Series in Computational Mathematics. Springer-Verlag; 1992. https://books.google.de/books?id=hg-oAAAAIAAJ.
3. Delfour MC, Zolésio JP. *Shapes and Geometries*, 2nd. Society for Industrial and Applied Mathematics; 2011. https://arxiv.org/abs/https://epubs.siam.org/doi/pdf/10.1137/1.9780898719826
4. Schulz V, Siebenborn M, Welker K. Efficient pde constrained shape optimization based on Steklov–Poincaré-type metrics. *SIAM J Optim*. 2016;26:2800-2819. doi:10.1137/15M1029369
5. Schulz V, Siebenborn M, Welker K. Structured inverse modeling in parabolic diffusion processess. *SIAM J Control Optim*. 2014;53:3319-3338. doi:10.1137/140985883
6. Azerad P, Ivorra B, Mohammadi B, Bouchette F. Optimal shape design of coastal structures minimizing Coastal Erosion; Vol. 1, 2005.
7. Isebe D, Azerad P, Bouchette F, Ivorra B, Mohammadi B. Shape optimization of geotextile tubes for sandy beach protection. *Int J Numer Methods Eng*. 2008;74:1262-1277. doi:10.1002/nme.2209
8. Keuthen M, Kraft D. Shape optimization of a breakwater. *Inverse Probl Sci Eng*. 2015;24:936-956. doi:10.1080/17415977.2015.1077522
9. Mohammadi B, Bouharguane A. Optimal dynamics of soft shapes in shallow waters. *Comput Fluids*. 2011;40:291-298. doi:10.1016/j.compfluid.2010.09.031
10. Bouharguane A, Mohammadi B. Minimization principles for the evolution of a soft sea bed interacting with a shallow. *Int J Comput Fluid Dyn*. 2012;26:163-172. doi:10.1080/10618562.2012.669831
11. Schlegel L, Schulz V. Shape optimization for the mitigation of coastal erosion via shallow water equations; 2021. https://arxiv.org/abs/2107.09464.
12. Barré de Saint-Venant A-J-C. Théorie du mouvement non-permanent des eaux, avec application aux crues des rivières et è l'introduction des marées dans leur lit. *Academic de Sci. Comptes Redus*. 1871;73(99):148-154.
13. Dewals B, Bruwier M, Pirotton M, Erpicum S, Archambeau P. Porosity models for large-scale urban flood modelling: a review. *Water*. 2021;13:960. doi:10.3390/w13070960
14. Guinot V, Soares-Frazão S. Flux and source term calculation in two-dimensional shallow water models with porosity on unstructured grids. *Int J Numer Methods Fluids*. 2006;50:309-345. doi:10.1002/fld.1059
15. Sanders BF, Schubert JE, Gallegos HA. Integral formulation of shallow-water equations with anisotropic porosity for urban flood modeling. *J Hydrol*. 2008;362:19-38. doi:10.1016/j.jhydrol.2008.08.009
16. Özgen I, Liang D, Hinkelmann R. Shallow water equations with depth-dependent anisotropic porosity for subgrid-scale topography. *Appl Math Model*. 2016;40:7447-7473. doi:10.1016/j.apm.2015.12.012
17. Hartmann R. Numerical analysis of higher order discontinuous Galerkin finite element methods; 2008.
18. Xing Y, Shu C-W. A new approach of high order well-balanced finite volume WENO schemes and discontinuous Galerkin methods for a class of hyperbolic systems with source. *Commun Comput Phys*. 2006;1:100-134.
19. Persson P-O, Peraire J. Sub-cell shock capturing for discontinuous Galerkin methods. *AIAA Pap*. 2006;2. doi:10.2514/6.2006-112
20. Oliger J, Sundström A. Theoretical and practical aspects of some initial boundary value problems in fluid dynamics. *SIAM J Appl Math*. 1978;35:419-446. doi:10.1137/0135035
21. Guba O, Taylor M, Ullrich P, Overfelt J, Levy M. The spectral element method (sem) on variable-resolution grids: evaluating grid sensitivity and resolution-aware numerical viscosity. *Geosci Model Dev Discuss*. 2014;7:2803-2816. doi:10.5194/gmdd-7-4081-2014
22. Song T, Main A, Scovazzi G, Ricchiuto M. The shifted boundary method for hyperbolic systems: embedded domain computations of linear waves and shallow water flows. *J Comput Phys*. 2017;12:45-79.

23. Allaire G, Jouve F, Michailidis G. Thickness control in structural optimization via a level set method. *Struct Multidiscip Optim*. 2016;53:1349-1382. doi:10.1007/s00158-016-1453-y
24. De los Reyes J. Numerical PDE-constrained optimization; Vol. 03, 2015. 10.1007/978-3-319-13395-9
25. Exner F. Über die Wechselwirkung zwischen Wasser und Geschiebe in Flüssen: Gedr. mit Unterstütztg aus d. Jerome u. Margaret Stonborough-Fonds, Hölder-Pichler-Tempsky, A.-G; 1925. https://books.google.de/books?id=7bjqZwEACAAJ
26. Berggren M. A unified discrete–Continuous sensitivity analysis method for shape optimization. *Applied and Numerical Partial Differential Equations*. Vol 15. Springer; 2010:25-39. doi:10.1007/978-90-481-3239-3_4
27. Alnæs MS, Blechta J, Hake J, et al. The FENICS project version 1.5. *Arch Numer Softw*. 2015;3:100. doi:10.11588/ans.2015.100.20553
28. Hairer E, Wanner G. Solving ordinary differential equations II. *Stiff Differ Algebraic Probl*. 1996;14:01. doi:10.1007/978-3-662-09947-6
29. Houston P, Sime N. Automatic symbolic computation for discontinuous Galerkin finite element methods; 2018. https://arxiv.org/abs/1804.02338.
30. Aizinger V, Dawson C. A discontinuous Galerkin method for two-dimensional flow and transport in shallow water. *Adv Water Resour*. 2002;25:67-84. doi:10.1016/S0309-1708(01)00019-7
31. Gosse L. A well-balanced flux-vector splitting scheme designed for hyperbolic systems of conservation laws with source terms. *Comput Math Appl*. 2000;39:135-159. doi:10.1016/S0898-1221(00)00093-6
32. Bermudez A, Vazquez ME. Upwind methods for hyperbolic conservation laws with source terms. *Comput Fluids*. 1994;23:1049-1071. doi:10.1016/0045-7930(94)90004-3
33. Audusse E, Chalons C, Ung P. A simple three-wave approximate Riemann solver for the Saint-Venant–Exner equations. *Int J Numer Methods Fluids*. 2015;87:508-528. doi:10.1002/fld.4500
34. Geuzaine C, Remacle J-F. Gmsh: a 3-D finite element mesh generator with built-in pre- and post-processing facilities. *Int J Numer Methods Eng*. 2009;79:1309-1331. doi:10.1002/nme.2579
35. Stefanakis TS, Contal E, Vayatis N, Dias F, Synolakis C. Can small islands protect nearby coasts from tsunamis? An active experimental design approach. *Proc Royal Soc A Math Phys Eng Sci*. 2014;470:20140575. doi:10.1098/rspa.2014.0575
36. Avdis A, Jacobs C, Mouradian S, Hill J, Piggott M. Meshing ocean domains for coastal engineering applications. Proceedings of the VII European Congress on Computational Methods in Applied Sciences and Engineering; Vol. 06, 2016, 10.7712/100016.1830.7712
37. Agoshkov V, Quarteroni A, Saleri F. Recent developments in the numerical simulation of shallow water equations I: boundary conditions. *Appl Numer Math*. 1994;15:175-200. doi:10.1016/0168-9274(94)00014-X
38. Correa R, Seeger A. Directional derivative of a minmax function. *Nonlinear Anal Theory Methods Appl*. 1985;9:13-22. doi:10.1016/0362-546X(85)90049-5

How to cite this article: Schlegel L, Schulz V. Shape optimization for the mitigation of coastal erosion via porous shallow water equations. *Int J Numer Methods Eng*. 2022;123(22):5416-5441. doi: 10.1002/nme.7074

APPENDIX A. DERIVATION OF VISCOUS POROUS MOMENTUM

We hereby follow Reference 14 and extend for diffusive terms. In addition, we assume a water density $\rho = 1$ and remark that the volume V of water in a control volume is given by

$$V = \int_{y_0}^{y_0+\delta y} \int_{x_0}^{x_0+\delta x} \phi H \, \mathrm{d}x \, \mathrm{d}y \tag{A1}$$

with x_0, y_0 being the coordinates of the lower left corner of the control volume. Following Reference 14, the momentum balance in x-direction can be written as

$$M = \frac{\partial M_x}{\partial t} - F_{M,W} + F_{M,E} - F_{M,S} + F_{M,N} - P_W + P_E - W_x - B_x - R_x = 0, \tag{A2}$$

where F-terms account for x-momentum fluxes, P-terms for pressure forces, such as W, B, and R-terms for porosity influence such as bottom pressure and friction terms with indices representing the western W, eastern E, northern N, and southern S sides of the control volume. For viscous SWE as in Reference 37, this momentum balance is extended by the volume diffusion through the western and eastern side as

$$D_W = -\int_{y_0}^{y_0+\delta y} \mu \phi H u_x(x_0, y) \, \mathrm{d}y, \tag{A3}$$

$$D_E = -\int_{y_0}^{y_0+\delta y} \mu\phi H u_x(x_0+\delta x, y)\,\mathrm{d}y \tag{A4}$$

such as southern and northern sides

$$D_S = -\int_{x_0}^{x_0+\delta x} \mu\phi H u_y(x, y_0)\,\mathrm{d}x, \tag{A5}$$

$$D_N = -\int_{x_0}^{x_0+\delta x} \mu\phi H u_y(x, y_0+\delta y)\,\mathrm{d}x, \tag{A6}$$

where u_x and u_y denote the first spatial derivatives with respect to x and y and diffusion coefficient μ. Momentum balancing these terms then leads to

$$M - D_W + D_E - D_S + D_N = 0. \tag{A7}$$

Substituting terms in (A7) gives

$$\begin{aligned} M &+ \int_{y_0}^{y_0+\delta y} \mu\phi H u_x(x_0, y)\,\mathrm{d}y - \int_{y_0}^{y_0+\delta y} \mu\phi H u_x(x_0+\delta x, y)\,\mathrm{d}y \\ &+ \int_{x_0}^{x_0+\delta x} \mu\phi H u_y(x, y_0)\,\mathrm{d}x - \int_{x_0}^{x_0+\delta x} \mu\phi H u_y(x, y_0+\delta y)\,\mathrm{d}x = 0. \end{aligned} \tag{A8}$$

When δx and analogously δy tend to 0, it holds

$$\lim_{\delta x\to 0} (\mu\phi H u_x)(x_0+\delta x, y) - (\mu\phi H u_x)(x_0, y) = \delta x \frac{\partial}{\partial x}(\mu\phi H u_x) \tag{A9}$$

such that an evaluation of integrals in (A8) yields

$$\delta x\delta y M - \delta x\delta y \frac{\partial}{\partial x}(\mu\phi H u_x) - \delta x\delta y \frac{\partial}{\partial y}(\mu\phi H u_y) = 0, \tag{A10}$$

which gives the momentum balance as

$$M - \frac{\partial}{\partial x}(\mu\phi H u_x) - \frac{\partial}{\partial y}(\mu\phi H u_y) = 0. \tag{A11}$$

The y-momentum is derived in accordance.

APPENDIX B. DERIVATION OF ADJOINT EQUATIONS

Proof. We perform integration by parts once more on time and spatial derivatives of the weak form (37), where boundaries are denoted as in Section 2, to obtain

$$\begin{aligned} a(H, \vec{Q}, p, \vec{r}) = &\int_0^T \int_\Omega -\frac{\partial p}{\partial t}\phi H\,\mathrm{d}x\,\mathrm{d}t + \int_\Omega \phi\left[H(T,x)p(T,x) - H_0 p(0,x)\right]\,\mathrm{d}x \\ &+ \int_0^T \int_\Omega -\phi\vec{Q}\cdot\nabla p\,\mathrm{d}x\,\mathrm{d}t + \int_0^T \int_{\Gamma_{\text{out}}} p\phi\vec{Q}\cdot\vec{n}\,\mathrm{d}s\,\mathrm{d}t \\ &+ \int_0^T \int_{\Gamma_3} [\![p\phi\vec{Q}\cdot\vec{n}]\!]\,\mathrm{d}s\,\mathrm{d}t \\ &+ \int_0^T \int_\Omega -(H+z)\nabla\cdot(\mu_v\nabla p)\,\mathrm{d}x\,\mathrm{d}t \\ &+ \int_0^T \int_{\Gamma_{\text{out}}} \left[\mu_v(H+z)\nabla p\cdot\vec{n} - p\mu_v\nabla(H+z)\cdot\vec{n}\right]\,\mathrm{d}s\,\mathrm{d}t \\ &+ \int_0^T \int_{\Gamma_3} \left[[\![\mu_v\nabla(H+z)\cdot\vec{n}p]\!] - [\![\mu_v(H+z)\nabla p\cdot\vec{n}]\!]\right]\,\mathrm{d}s\,\mathrm{d}t \end{aligned}$$

$$
\begin{aligned}
&+\int_0^T\int_\Omega -\frac{\partial \vec{r}}{\partial t}\cdot(\phi\vec{Q})\,\mathrm{d}x\,\mathrm{d}t+\int_\Omega \phi\left[\vec{Q}(T,x)\cdot\vec{r}(T,x)-\vec{Q}_0\cdot\vec{r}(0,x)\right]\,\mathrm{d}x\\
&+\int_0^T\int_\Omega -\phi\frac{\vec{Q}}{H}\cdot\nabla\vec{r}\cdot\vec{Q}\,\mathrm{d}x\,\mathrm{d}t+\int_0^T\int_{\Gamma_{\text{out}}}\phi\frac{\vec{Q}}{H}\cdot\vec{r}\vec{Q}\cdot\vec{n}\,\mathrm{d}s\,\mathrm{d}t\\
&+\int_0^T\int_\Omega -\frac{1}{2}g\phi H^2\nabla\cdot\vec{r}\,\mathrm{d}x\,\mathrm{d}t+\int_0^T\int_{\Gamma_{\text{out}}}\frac{1}{2}g\phi H^2\vec{r}\cdot\vec{n}\,\mathrm{d}s\,\mathrm{d}t\\
&+\int_0^T\int_{\Gamma_3}\left[\!\!\left[\phi\frac{\vec{Q}}{H}\cdot\vec{r}\vec{Q}\cdot\vec{n}\right]\!\!\right]\,\mathrm{d}s\,\mathrm{d}t+\int_0^T\int_{\Gamma_3}\left[\!\!\left[\frac{1}{2}g\phi H^2\vec{r}\cdot\vec{n}\right]\!\!\right]\,\mathrm{d}s\,\mathrm{d}t\\
&+\int_0^T\int_\Omega -\vec{Q}\cdot\nabla\cdot(\mu_f\phi\nabla\vec{r})\,\mathrm{d}x\,\mathrm{d}t+\int_0^T\int_\Omega g\phi H\nabla z\cdot\vec{r}\,\mathrm{d}x\,\mathrm{d}t\\
&+\int_0^T\int_\Gamma\left[\mu_f\phi\vec{Q}\cdot\nabla\vec{r}\cdot\vec{n}-\vec{r}\cdot(\mu_f\phi\nabla\vec{Q})\cdot\vec{n}\right]\,\mathrm{d}s\,\mathrm{d}t\\
&+\int_0^T\int_{\Gamma_3}\left[[\![\mu_f\phi\nabla(\vec{Q})\cdot\vec{n}\cdot\vec{r}]\!]-[\![\mu_f\phi\nabla\vec{r}\cdot\vec{Q}\cdot\vec{n}]\!]\right]\,\mathrm{d}s\,\mathrm{d}t\\
&-\int_0^T\int_\Omega g\frac{1}{2}H^2\nabla\phi\cdot\vec{r}\,\mathrm{d}s\,\mathrm{d}t. \qquad \text{(B1)}
\end{aligned}
$$

Using the jump identity $[\![ab]\!]=\{\{a\}\}[\![b]\!]+\{\{b\}\}[\![a]\!]$ on boundary integrals over the interface Γ_3 and inserting Boundary Conditions (6) on Γ_1 and Γ_2 for terms that arise from the diffusive fluxes lead to

$$
\begin{aligned}
a(H,\vec{Q},p,\vec{r})=&\int_0^T\int_\Omega -\frac{\partial p}{\partial t}\phi H\,\mathrm{d}x\,\mathrm{d}t+\int_\Omega\phi\left[H(T,x)p(T,x)-H_0p(0,x)\right]\,\mathrm{d}x\\
&-\int_0^T\int_\Omega\phi\vec{Q}\cdot\nabla p\,\mathrm{d}x\,\mathrm{d}t+\int_0^T\int_{\Gamma_2}\phi p\vec{Q}\cdot\vec{n}\,\mathrm{d}s\,\mathrm{d}t\\
&+\int_0^T\int_{\Gamma_3}[\![p\phi\vec{Q}\cdot\vec{n}]\!]\,\mathrm{d}s\,\mathrm{d}t-\int_0^T\int_\Omega\frac{1}{2}g\phi H^2\nabla\cdot\vec{r}\,\mathrm{d}x\,\mathrm{d}t\\
&-\int_0^T\int_\Omega(H+z)\nabla\cdot(\mu_v\nabla p)\,\mathrm{d}x\,\mathrm{d}t+\int_0^T\int_{\Gamma_1}\mu_v(H+z)\nabla p\cdot\vec{n}\,\mathrm{d}s\,\mathrm{d}t\\
&+\int_0^T\int_{\Gamma_2}\mu_vH_1\nabla p\cdot\vec{n}\,\mathrm{d}s\,\mathrm{d}t+\int_0^T\int_{\Gamma_2}-p\mu_v\nabla(H_1+z)\cdot\vec{n}\,\mathrm{d}s\,\mathrm{d}t\\
&+\int_0^T\int_{\Gamma_3}\left[\{\{\mu_v\nabla(H+z)\cdot\vec{n}\}\}[\![p]\!]-\{\{H+z\}\}[\![\mu_v\nabla p\cdot\vec{n}]\!]\right]\,\mathrm{d}s\,\mathrm{d}t\\
&-\int_0^T\int_\Omega\frac{\partial\vec{r}}{\partial t}\cdot(\phi\vec{Q})\,\mathrm{d}x\,\mathrm{d}t+\int_\Omega\phi\left[\vec{Q}(T,x)\cdot\vec{r}(T,x)-\vec{Q}_0\cdot\vec{r}(0,x)\right]\,\mathrm{d}x\\
&-\int_0^T\int_\Omega\phi\frac{\vec{Q}}{H}\cdot\nabla\vec{r}\cdot\vec{Q}\,\mathrm{d}x\,\mathrm{d}t+\int_0^T\int_{\Gamma_2}\phi\frac{\vec{Q}}{H_1}\cdot\vec{r}\vec{Q}\cdot\vec{n}\,\mathrm{d}s\,\mathrm{d}t\\
&+\int_0^T\int_{\Gamma_1}\frac{1}{2}g\phi H^2\vec{r}\cdot\vec{n}\,\mathrm{d}s\,\mathrm{d}t+\int_0^T\int_{\Gamma_2}\frac{1}{2}g\phi H_1^2\vec{r}\cdot\vec{n}\,\mathrm{d}s\,\mathrm{d}t\\
&+\int_0^T\int_{\Gamma_3}\left[\!\!\left[\phi\frac{\vec{Q}}{H}\cdot\vec{r}\vec{Q}\cdot\vec{n}\right]\!\!\right]\,\mathrm{d}s\,\mathrm{d}t+\int_0^T\int_{\Gamma_3}\left[\!\!\left[\frac{1}{2}g\phi H^2\vec{r}\cdot\vec{n}\right]\!\!\right]\,\mathrm{d}s\,\mathrm{d}t\\
&-\int_0^T\int_\Omega(\vec{Q})\cdot\nabla\cdot(\mu_f\phi\nabla\vec{r})\,\mathrm{d}x\,\mathrm{d}t+\int_0^T\int_{\Gamma_1,\Gamma_2}\mu_f\phi\vec{Q}\nabla\vec{r}\cdot\vec{n}\,\mathrm{d}s\,\mathrm{d}t\\
&+\int_0^T\int_{\Gamma_3}\left[\{\{\mu_f\phi\nabla(\vec{Q})\cdot\vec{n}\}\}\cdot[\![\vec{r}]\!]-\{\{\vec{Q}\}\}\cdot[\![\mu_f\phi\nabla\vec{r}\cdot\vec{n}]\!]\right]\,\mathrm{d}s\,\mathrm{d}t\\
&+\int_0^T\int_\Omega g\phi H\nabla z\cdot\vec{r}\,\mathrm{d}x\,\mathrm{d}t-\int_0^T\int_\Omega g\frac{1}{2}H^2\nabla\phi\cdot\vec{r}\,\mathrm{d}x\,\mathrm{d}t. \qquad \text{(B2)}
\end{aligned}
$$

Differentiating for the state variable H leads to

$$\begin{aligned}\frac{\partial a(H,\vec{Q},p,\vec{r})}{\partial H} &= \int_0^T\int_\Omega -\frac{\partial \phi p}{\partial t}\,\mathrm{d}x\,\mathrm{d}t + \int_\Omega \phi p(T,x)\,\mathrm{d}x \\ &+ \int_0^T\int_\Omega -\nabla\cdot(\mu_v\nabla p)\,\mathrm{d}x\,\mathrm{d}t + \int_0^T\int_{\Gamma_1}\left[\mu_v\nabla p\cdot\vec{n}\right]\,\mathrm{d}s\,\mathrm{d}t \\ &+ \int_0^T\int_{\Gamma_3}\left[\{\{\mu_v\nabla(H+z)\cdot\vec{n}\}\}_H[\![p]\!] - \{\{H+z\}\}_H[\![\mu_v\nabla p\cdot\vec{n}]\!]\right]\,\mathrm{d}s\,\mathrm{d}t \\ &- \int_0^T\int_\Omega \phi\frac{\vec{Q}}{H^2}\cdot\nabla\vec{r}\cdot\vec{Q}\,\mathrm{d}x\,\mathrm{d}t \\ &- \int_0^T\int_{\Gamma_3}\left[\!\!\left[\phi\frac{\vec{Q}}{H^2}\cdot\vec{r}\vec{Q}\cdot\vec{n}\right]\!\!\right]\,\mathrm{d}s\,\mathrm{d}t + \int_0^T\int_{\Gamma_3}[\![g\phi H\vec{r}\cdot\vec{n}]\!]\,\mathrm{d}s\,\mathrm{d}t \\ &- \int_0^T\int_\Omega -g\phi H\nabla\cdot\vec{r}\,\mathrm{d}x\,\mathrm{d}t + \int_0^T\int_{\Gamma_1} g\phi H\vec{r}\cdot\vec{n}\,\mathrm{d}s\,\mathrm{d}t \\ &+ \int_0^T\int_\Omega g\phi\nabla z\cdot\vec{r}\,\mathrm{d}x\,\mathrm{d}t - \int_0^T\int_\Omega gH\nabla\phi\cdot\vec{r}\,\mathrm{d}x\,\mathrm{d}t \end{aligned} \tag{B3}$$

and w.r.t. $\vec{Q}$ to

$$\begin{aligned}\frac{\partial a(H,\vec{Q},p,\vec{r})}{\partial \vec{Q}} &= \int_0^T\int_\Omega -\frac{\partial\phi\vec{r}}{\partial t}\,\mathrm{d}x\,\mathrm{d}t + \int_\Omega \phi\vec{r}(T,x)\,\mathrm{d}x \\ &- \int_0^T\int_\Omega \phi\nabla p\,\mathrm{d}x\,\mathrm{d}t + \int_0^T\int_{\Gamma_2}\phi p\vec{n}\,\mathrm{d}s\,\mathrm{d}t + \int_0^T\int_{\Gamma_3}[\![p\phi\vec{n}]\!] \\ &\times\int_0^T\int_\Omega -\phi\frac{1}{H}(\nabla\vec{r})^T\vec{Q} - \frac{1}{H}(\vec{Q}\cdot\nabla)\vec{r}\vec{Q}\,\mathrm{d}x\,\mathrm{d}t \\ &+ \int_0^T\int_{\Gamma_2}\frac{\phi}{H_1}(\vec{Q}\cdot\vec{n})\vec{r}\,\mathrm{d}s\,\mathrm{d}t + \int_0^T\int_{\Gamma_2}\frac{\phi}{H_1}(\vec{Q}\vec{r})\cdot\vec{n}\,\mathrm{d}s\,\mathrm{d}t \\ &+ \int_0^T\int_{\Gamma_3}\left[\!\!\left[\frac{\phi}{H}(\vec{Q}\cdot\vec{n})\vec{r}\right]\!\!\right]\,\mathrm{d}s\,\mathrm{d}t + \int_0^T\int_{\Gamma_3}\left[\!\!\left[\frac{\phi}{H}(\vec{Q}\vec{r})\cdot\vec{n}\right]\!\!\right]\,\mathrm{d}s\,\mathrm{d}t \\ &- \int_0^T\int_\Omega \nabla\cdot(\mu_f\phi\nabla\vec{r})\,\mathrm{d}x\,\mathrm{d}t + \int_0^T\int_{\Gamma_1,\Gamma_2}\mu_f\phi\nabla\vec{r}\vec{n}\,\mathrm{d}s\,\mathrm{d}t \\ &+ \int_0^T\int_{\Gamma_3}\left[\{\{\mu_f\phi\nabla(\vec{Q})\vec{n}\}\}_{\vec{Q}}[\![\vec{r}]\!] - \{\{\vec{Q}\}\}_{\vec{Q}}[\![\mu_f\phi\nabla\vec{r}\vec{n}]\!]\right]\,\mathrm{d}s\,\mathrm{d}t, \end{aligned} \tag{B4}$$

where the subscript denotes differentiation for the respective state variable. Now if $\frac{\partial a(H,\vec{Q},p,\vec{r})}{\partial U} = -\frac{\partial J_1}{\partial U}$ then $\frac{\partial \mathcal{L}}{\partial U} = 0$ is fulfilled. From this we get the adjoint equations in strong form (38) and (39) with boundary conditions from equating boundary terms to zero in (B3) and (B4). ∎

APPENDIX C. DERIVATION OF SHAPE DERIVATIVE

Proof. We regard the Lagrangian (36). As in Reference 5, the theorem of Correa and Seger[38] is applied on the right-hand side of

$$J_1(\Omega) = \min_U \max_P \mathcal{L}(\Omega, U, P). \tag{C1}$$

The assumptions of this theorem can be verified as in Reference 3. We now use the definition of the shape derivative (27) in terms of the Lagrangian, that is,

$$\begin{aligned} D\mathcal{L}(\Omega,U,P)[\vec{V}] &= \lim_{\epsilon\to 0^+}\frac{\mathcal{L}(\Omega_\epsilon;U,P) - \mathcal{L}(\Omega;U,P)}{\epsilon} \\ &= \frac{d}{d\epsilon}\,\mathcal{L}(\Omega_\epsilon,U,P)\big|_{\epsilon=0^+} = \frac{d}{d\epsilon}\,\mathcal{L}(\Omega_\epsilon,H,\vec{Q},p,\vec{r})\Big|_{\epsilon=0^+} \end{aligned}$$

and apply the rule for differentiating domain integrals (35), where we split integrals for readability in to be added domain part, that is,

$$\begin{aligned}
&\int_\Omega \Bigg[\int_0^T - D_m\left(\frac{\partial p}{\partial t}\phi H\right)\,\mathrm{d}t + D_m\left(\phi H(T,x)p(T,x) - \phi H_0 p(0,x)\right) \\
&\quad + \int_0^T - D_m\left(\frac{\partial \vec{r}}{\partial t}\cdot\phi\vec{Q}\right)\,\mathrm{d}t + D_m\left(\phi\vec{Q}(T,x)\cdot\vec{r}(T,x) - \phi\vec{Q}_0\cdot\vec{r}(0,x)\right) \\
&\quad + \int_0^T D_m\left(\nabla\cdot(\phi\vec{Q})p\right)\,\mathrm{d}t + \int_0^T D_m\left(\mu_v\nabla(H+z)\cdot\nabla p\right)\,\mathrm{d}t \\
&\quad + \int_0^T D_m\left(\nabla\cdot\left(\phi\frac{\vec{Q}}{H}\otimes\vec{Q}\right)\cdot\vec{r}\right)\,\mathrm{d}t + \int_0^T + D_m\left(\frac{1}{2}g\nabla(\phi H^2)\cdot\vec{r}\right)\,\mathrm{d}t \\
&\quad + \int_0^T D_m\left(\phi\mu_f\nabla\vec{Q} : \nabla\vec{r}\right)\,\mathrm{d}t + \int_0^T D_m\left(gH\nabla z\cdot\vec{r}\right)\,\mathrm{d}t \\
&\quad + \int_0^T - D_m\left(\frac{1}{2}gH^2\nabla\phi\cdot\vec{r}\right)\,\mathrm{d}t \\
&\quad + \mathrm{div}(\vec{V})\left(\int_0^T - \frac{\partial p}{\partial t}\phi H\,\mathrm{d}t + \phi H(T,x)p(T,x) - \phi H_0 p(0,x)\right. \\
&\quad + \int_0^T - \frac{\partial\vec{r}}{\partial t}\cdot(\phi\vec{Q})\,\mathrm{d}t + \phi\vec{Q}(T,x)\cdot\vec{r}(T,x) - \phi\vec{Q}_0\cdot\vec{r}(0,x) + \int_0^T \nabla\vec{Q}\cdot p\,\mathrm{d}t \\
&\quad + \int_0^T \mu_v\nabla(H+z)\cdot\nabla p\,\mathrm{d}t + \int_0^T \nabla\cdot\left(\phi\frac{\vec{Q}}{H}\otimes\vec{Q}\right)\cdot\vec{r}\,\mathrm{d}t \\
&\quad + \int_0^T + \frac{1}{2}g\nabla(\phi H^2)\cdot\vec{r}\,\mathrm{d}t + \int_0^T \phi\mu_f\nabla\vec{Q} : \nabla\vec{r}\,\mathrm{d}t + \int_0^T g\phi H\nabla z\cdot\vec{r}\,\mathrm{d}t \\
&\quad \left. - \int_0^T gH^2\nabla\phi\cdot\vec{r}\,\mathrm{d}t\right)\Bigg]\,\mathrm{d}x
\end{aligned}$$

and interior such as exterior boundary part, that is,

$$\begin{aligned}
&\int_{\Gamma_1}\left[\frac{1}{2}\int_0^T D_m\left([N(\hat{U}(t,x)-\bar{U}(t,x))]^2\right) + \mathrm{div}_{\Gamma_1}(\vec{V})[N(\hat{U}(t,x)-\bar{U}(t,x))]^2\,\mathrm{d}t\right]\,\mathrm{d}s \\
&\quad - \int_{\Gamma_2}\left[\int_0^T D_m\left(\mu_v\nabla(H_1+z)\cdot\vec{n}p\,\mathrm{d}t\right) + \mathrm{div}_{\Gamma_2}(\vec{V})\left(\int_0^T \mu_v\nabla(H_1+z)\cdot\vec{n}p\,\mathrm{d}t\right)\right]\,\mathrm{d}s \\
&\quad - \int_{\Gamma_3}\left[\int_0^T D_m\left([\![\mu_v\nabla(H+z)\cdot\vec{n}p]\!]\right)\,\mathrm{d}t + \int_0^T D_m\left([\![\phi\mu_f\nabla\vec{Q}\cdot\vec{n}\cdot\vec{r}]\!]\right)\,\mathrm{d}t\right. \\
&\quad \left. + \mathrm{div}_{\Gamma_3}(\vec{V})\left(\int_0^T [\![-\mu_v\nabla(H+z)\cdot\vec{n}p]\!]\,\mathrm{d}t + \int_0^T [\![-\phi\mu_f\nabla\vec{Q}\cdot\vec{n}\cdot\vec{r}]\!]\,\mathrm{d}t\right)\right]\,\mathrm{d}s,
\end{aligned}$$

where $\mathrm{div}_\Gamma(\vec{V}) = \mathrm{div}(\vec{V}) - \vec{n}\cdot(\nabla\vec{V})\vec{n}$ is the tangential divergence of the vector field $\vec{V}$ for the respective boundary normal $\vec{n}$. Now the product rule (31) yields, respectively, for the domain part

$$\begin{aligned}
&= \int_\Omega\left[\int_0^T - D_m\left(\frac{\partial p}{\partial t}\right)\phi H - \frac{\partial p}{\partial t}D_m(\phi H)\,\mathrm{d}t\right. \\
&\quad + D_m(\phi H(T,x))p(T,x) + H(T,x)\dot{p}(T,x) - \phi H_0\dot{p}(0,x) \\
&\quad + \int_0^T - D_m\left(\frac{\partial\vec{r}}{\partial t}\right)\cdot(\phi\vec{Q}) - \frac{\partial\vec{r}}{\partial t}\cdot D_m(\phi\vec{Q})\,\mathrm{d}t + D_m(\vec{Q}(T,x))\cdot\vec{r}(T,x) \\
&\quad + \phi\vec{Q}(T,x)\cdot\dot{\vec{r}}(T,x) - \phi\vec{Q}_0\cdot\dot{\vec{r}}(0,x) + \int_0^T \dot{p}\cdot\nabla(\phi\vec{Q}) + p\cdot D_m(\nabla(\phi\vec{Q}))\,\mathrm{d}t \\
&\quad \left. + \int_0^T (\mu_v D_m(\nabla(H+z))\cdot\nabla p + \mu_v\nabla(H+z)\cdot D_m(\nabla p))\,\mathrm{d}t\right.
\end{aligned}$$

$$
\begin{aligned}
&- \int_0^T D_m\left(\nabla\cdot\left(\phi\frac{\vec{Q}}{H}\otimes\vec{Q}\right)\right)\cdot\vec{r}\,\mathrm{d}t + \int_0^T \nabla\cdot\left(\phi\frac{\vec{Q}}{H}\otimes\vec{Q}\right)\cdot D_m\left(\vec{r}\right)\,\mathrm{d}t\\
&+ \int_0^T \left(\frac{1}{2}gD_m(\nabla(\phi H^2))\cdot\vec{r} + \frac{1}{2}g\nabla(\phi H^2)\cdot D_m(\vec{r})\right)\,\mathrm{d}t\\
&+ \int_0^T \left(D_m\left(\phi\mu_f\nabla\vec{Q}\right) : \nabla\vec{r} + \phi\mu_f\nabla\vec{Q} : D_m\left(\nabla\vec{r}\right)\right)\,\mathrm{d}t\\
&+ \int_0^T gD_m(\phi H)\nabla z\cdot\vec{r}\,\mathrm{d}t + \int_0^T g\phi H D_m\left(\nabla z\right)\cdot\vec{r}\,\mathrm{d}t + \int_0^T g\phi H\nabla z\cdot\dot{\vec{r}}\,\mathrm{d}t\\
&- \int_0^T \frac{1}{2}gD_m(H^2)\nabla\phi\cdot\vec{r}\,\mathrm{d}t - \int_0^T \frac{1}{2}gH^2D_m\left(\nabla\phi\right)\cdot\vec{r}\,\mathrm{d}t - \int_0^T \frac{1}{2}gH^2\nabla\phi\cdot\dot{\vec{r}}\,\mathrm{d}t\\
&+ \operatorname{div}(\vec{V})\left(\int_0^T -\frac{\partial p}{\partial t}\phi H\,\mathrm{d}t + \phi H(T,x)p(T,x) - \phi H_0p(0,x)\right.\\
&+ \int_0^T -\frac{\partial\vec{r}}{\partial t}\cdot(\phi\vec{Q})\,\mathrm{d}t + \phi\vec{Q}(T,x)\cdot\vec{r}(T,x) - \phi\vec{Q}_0\cdot\vec{r}(0,x) + \int_0^T \nabla\vec{Q}\cdot p\,\mathrm{d}t\\
&+ \int_0^T \mu_v\nabla(H+z)\cdot\nabla p\,\mathrm{d}t + \int_0^T \nabla\cdot\left(\phi\frac{\vec{Q}}{H}\otimes\vec{Q}\right)\cdot\vec{r}\,\mathrm{d}t\\
&+ \int_0^T \frac{1}{2}g\nabla(\phi H^2)\cdot\vec{r}\,\mathrm{d}t + \int_0^T \phi\mu_f\nabla\vec{Q} : \nabla\vec{r}\,\mathrm{d}t + \int_0^T g\phi H\nabla z\cdot\vec{r}\,\mathrm{d}t\\
&\left.- \int_0^T gH^2\nabla\phi\cdot\vec{r}\,\mathrm{d}t\right)\Bigg]\,\mathrm{d}x
\end{aligned}
$$

and the boundary part

$$
\begin{aligned}
&\int_{\Gamma_1}\left[\int_0^T [N(\hat{U}(t,x)-\bar{U}(t,x))]\cdot\dot{\hat{U}}\,\mathrm{d}t\right.\\
&\left.+ \operatorname{div}_{\Gamma_1}(\vec{V})\left(\int_0^T [N(\hat{U}(t,x)-\bar{U}(t,x))]^2\,\mathrm{d}t\right)\right]\,\mathrm{d}s\\
&+ \int_{\Gamma_2}\left[\int_0^T -\mu_v\nabla(H_1+z)\cdot\vec{n}\dot{p}\,\mathrm{d}t\right.\\
&\left.+ \operatorname{div}_{\Gamma_2}(\vec{V})\left(\int_0^T -\mu_v\nabla(H_1+z)\cdot\vec{n}p\,\mathrm{d}t\right)\right]\,\mathrm{d}s\\
&+ \int_{\Gamma_3}\left[\int_0^T [\![-\mu_vD_m\left(\nabla(H+z)\right)\cdot\vec{n}p - \mu_v\nabla(H+z)\cdot\vec{n}\dot{p}]\!]\,\mathrm{d}t\right.\\
&+ \int_0^T [\![-\phi\mu_fD_m(\nabla\vec{Q}\cdot\vec{n})\cdot\vec{r} - \phi\mu_f\nabla\vec{Q}\cdot\vec{n}\cdot\dot{\vec{r}}]\!]\,\mathrm{d}t\\
&\left.+ \operatorname{div}_{\Gamma_3}(\vec{V})\left(\int_0^T [\![-\mu_v\nabla(H+z)\cdot\vec{n}p]\!]\,\mathrm{d}t + \int_0^T [\![-\phi\mu_f\nabla\vec{Q}\cdot\vec{n}\cdot\vec{r}]\!]\,\mathrm{d}t\right)\right]\,\mathrm{d}s.
\end{aligned}
$$

The combination of both integrals, the non-commuting of material and spatial derivatives (32)–(34), integration by parts combined with the fact that sediment and porosity move alongside with the deformation, which ultimately lets the material derivative vanish, such as finally regrouping for the material derivatives of the state $U = (H, \vec{Q})$ and adjoint variables $P = (p, \vec{r})$, lead to three parts, where first

$$
\begin{aligned}
&\int_{\Gamma_1}\int_0^T [N(\hat{U}(t,x)-\bar{U}(t,x))]\cdot\dot{U}\,\mathrm{d}t\,\mathrm{d}s\\
&+ \int_\Omega\int_0^T \left[\left(-\phi\frac{\partial p}{\partial t} + \frac{\phi}{H^2}(\vec{Q}\cdot\nabla)\vec{r}\cdot\vec{Q} - g\phi H(\nabla\cdot\vec{r}) - \nabla\cdot(\mu_v\nabla p) + g\phi\nabla z\cdot\vec{r}\right)\dot{H}\right.
\end{aligned}
$$

$$
\begin{aligned}
&+\left(-\phi\frac{\partial\vec{r}}{\partial t}-\nabla p-\frac{\phi}{H}(\vec{Q}\cdot\nabla)\vec{r}-\frac{\phi}{H}(\nabla\vec{r})^T\vec{Q}-(\nabla\cdot(\phi\mu_f\nabla\vec{r}))\right)\cdot\dot{\vec{Q}}\\
&+\left(\phi\frac{\partial H}{\partial t}+\nabla\cdot\left(\phi\vec{Q}-\mu_v\nabla(H+z)\right)\right)\dot{p}\\
&+\left(\phi\frac{\partial\vec{Q}}{\partial t}+\nabla\cdot\left(\phi\frac{\vec{Q}}{H}\otimes\vec{Q}+\frac{1}{2}g\phi H^2\mathbf{I}-\phi\mu_f\nabla\vec{Q}\right)+g\phi H\nabla z\right)\cdot\dot{\vec{r}}\,\mathrm{d}t\Bigg]\,\mathrm{d}x
\end{aligned}
$$

vanishes due to an evaluation the Lagrangian in its saddle point and second

$$
\begin{aligned}
&\int_{\Gamma_1}\int_0^T\left[\mathrm{div}_{\Gamma_1}(\vec{V})[N(\hat{U}(t,x)-\bar{U}(t,x))]^2\right]\,\mathrm{d}t\,\mathrm{d}s\\
&\quad+\int_{\Gamma_3}\Bigg[\int_0^T\Bigg([\![\frac{\dot{\phi\vec{Q}}}{H}\cdot\vec{r}\vec{Q}\cdot\vec{n}+\frac{\phi\vec{Q}}{H}\cdot\vec{r}\dot{\vec{Q}}\cdot\vec{n}+p\dot{\phi\vec{Q}}\cdot\vec{n}\\
&\quad+\int_0^T\frac{1}{2}gD_m(\phi H^2)\vec{r}\cdot\vec{n}]\!]\Bigg)\,\mathrm{d}t\Bigg]\,\mathrm{d}s\\
&\quad+\mathrm{div}_{\Gamma_3}(\vec{V})\left(\int_0^T[\![-\mu_v\nabla(H+z)\cdot\vec{n}p]\!]\,\mathrm{d}t+\int_0^T[\![-\phi\mu_f\nabla\vec{Q}\cdot\vec{n}\cdot\vec{r}]\!]\,\mathrm{d}t\right)\Bigg]\,\mathrm{d}s
\end{aligned}
$$

vanishes since on the one hand outer boundaries are not variable and hence the deformation field $\vec{V}$ vanishes in small neighborhoods around Γ_1,Γ_2 such that the material derivative is zero and on the other due the continuity of state and fluxes corresponding material derivatives are continuous. Finally, this leaves us with the shape derivative in its final form (53)

$$
\begin{aligned}
DJ_1(\Omega)[\vec{V}]=\int_0^T\int_\Omega\Bigg[&-(\nabla\vec{V})^T:\nabla(\phi\vec{Q})p-(\nabla\vec{V})^T:\nabla\vec{Q}\frac{\phi\vec{Q}}{H}\cdot\vec{r}\\
&-(\nabla\vec{V}\vec{Q}\cdot\nabla)\frac{\phi\vec{Q}}{H}\cdot\vec{r}-gH(\nabla\vec{V})^T\nabla(\phi H)\cdot\vec{r}\\
&-\mu_v\nabla(H+z)^T(\nabla\vec{V}+\nabla\vec{V}^T)\nabla p\\
&-\phi\mu_f\nabla\vec{Q}\nabla\vec{V}:\nabla\vec{r}-\phi\mu_f\nabla\vec{Q}\nabla\vec{V}^T:\nabla\vec{r}\\
&-g\phi H\nabla\vec{V}^T\nabla z\cdot\vec{r}+\frac{1}{2}gH^2\nabla\vec{V}^T\nabla\phi\cdot\vec{r}\\
&\times\mathrm{div}(\vec{V})\left\{\frac{\partial\phi H}{\partial t}p+\nabla\cdot(\phi\vec{Q})p+\frac{\partial\phi\vec{Q}}{\partial t}\cdot\vec{r}\right.\\
&+\phi(\vec{Q}\cdot\nabla)\frac{\vec{Q}}{H}\cdot\vec{r}+\nabla\cdot(\phi\vec{Q})\frac{\vec{Q}}{H}\cdot\vec{r}+\frac{1}{2}g\nabla(\phi H^2)\cdot\vec{r}\\
&+g\phi H\nabla z\cdot\vec{r}+\mu_v\nabla(H+z)\cdot\nabla p\\
&\left.+\ \phi\mu_f\nabla\vec{Q}:\nabla\vec{r}-g\frac{1}{2}H^2\nabla\phi\cdot\vec{r}\right\}\Bigg]\,\mathrm{d}x\,\mathrm{d}t.
\end{aligned}
$$

■

APPENDIX D. DERIVATION OF DG SCHEME FOR INTERFACE CONDITIONS

The porous SWE (1) together with interface conditions on Γ_3 can be resolved in an SIP-DG scheme. Starting from the weak form (37) and integrating by parts once more on the advective terms, in addition to once more using the jump identity $[\![ab]\!]=\{\{a\}\}[\![b]\!]+\{\{b\}\}[\![a]\!]$ together with flux continuity for the diffusive and advective flux we obtain

$$
a(H,\vec{Q},p,\vec{r})=\int_0^T\int_\Omega-\frac{\partial p}{\partial t}\phi H\,\mathrm{d}x\,\mathrm{d}t+\int_\Omega\phi\left[H(T,x)p(T,x)-H_0p(0,x)\right]\,\mathrm{d}x
$$

$$
\begin{aligned}
&+ \int_0^T \int_\Omega -\phi\vec{Q}\cdot\nabla p \,\mathrm{d}x\,\mathrm{d}t + \int_0^T \int_{\Gamma_{\text{out}}} p\phi\vec{Q}\cdot\vec{n}\,\mathrm{d}s\,\mathrm{d}t \\
&+ \int_0^T \int_{\Gamma_3} \{\{\phi\vec{Q}\cdot\vec{n}\}\}[\![p]\!]\,\mathrm{d}s\,\mathrm{d}t \\
&+ \int_0^T \int_\Omega \mu_v \nabla(H+z)\cdot\nabla p \,\mathrm{d}x\,\mathrm{d}t \\
&- \int_0^T \int_{\Gamma_{\text{out}}} \left[p\mu_v\nabla(H+z)\cdot\vec{n}\right]\,\mathrm{d}s\,\mathrm{d}t \\
&- \int_0^T \int_{\Gamma_3} \left[\{\{\mu_v\nabla(H+z)\cdot\vec{n}\}\}[\![p]\!]\right]\,\mathrm{d}s\,\mathrm{d}t \\
&- \int_0^T \int_\Omega -\frac{\partial\vec{r}}{\partial t}\cdot(\phi\vec{Q})\,\mathrm{d}x\,\mathrm{d}t + \int_\Omega \phi\left[\vec{Q}(T,x)\cdot\vec{r}(T,x) - \vec{Q}_0\cdot\vec{r}(0,x)\right]\,\mathrm{d}x \\
&+ \int_0^T \int_\Omega -\phi\frac{\vec{Q}}{H}\cdot\nabla\vec{r}\cdot\vec{Q}\,\mathrm{d}x\,\mathrm{d}t + \int_0^T \int_{\Gamma_{\text{out}}} \phi\frac{\vec{Q}}{H}\cdot\vec{r}\vec{Q}\cdot\vec{n}\,\mathrm{d}s\,\mathrm{d}t \\
&+ \int_0^T \int_\Omega -\frac{1}{2}g\phi H^2\nabla\cdot\vec{r}\,\mathrm{d}x\,\mathrm{d}t + \int_0^T \int_{\Gamma_{\text{out}}} \frac{1}{2}g\phi H^2\vec{r}\cdot\vec{n}\,\mathrm{d}s\,\mathrm{d}t \\
&+ \int_0^T \int_{\Gamma_3} \left\{\left\{\phi(\frac{\vec{Q}}{H}\otimes\vec{Q})\vec{n}\right\}\right\}\cdot[\![\vec{r}]\!]\,\mathrm{d}s\,\mathrm{d}t + \int_0^T \int_{\Gamma_3} \left\{\left\{\frac{1}{2}g\phi H^2\vec{n}\right\}\right\}\cdot[\![\vec{r}]\!]\,\mathrm{d}s\,\mathrm{d}t \\
&+ \int_0^T \int_\Omega \mu_f\phi\nabla\vec{Q} : \nabla\vec{r}\,\mathrm{d}x\,\mathrm{d}t + \int_0^T \int_\Omega g\phi H\nabla z\cdot\vec{r}\,\mathrm{d}x\,\mathrm{d}t \\
&- \int_0^T \int_\Gamma \left[\vec{r}\cdot\mu_f\phi\nabla\vec{Q}\cdot\vec{n}\right]\,\mathrm{d}s\,\mathrm{d}t \\
&- \int_0^T \int_{\Gamma_3} \left[\{\{\mu_f\phi\nabla\vec{Q}\cdot\vec{n}\}\}\cdot[\![\vec{r}]\!]\right]\,\mathrm{d}s\,\mathrm{d}t \\
&- \int_0^T \int_\Omega g\frac{1}{2}H^2\nabla\phi\cdot\vec{r}\,\mathrm{d}s\,\mathrm{d}t.
\end{aligned}
\tag{D1}
$$

Since this derivation does not make use of the continuity of the solutions (7)–(9), we weakly enforce it by adding

$$
\int_0^T \int_{\Gamma_3} \underline{\delta}(\hat{U}) : \underline{[\![P]\!]}\,\mathrm{d}s\,\mathrm{d}t \tag{D2}
$$

for

$$
\underline{\delta}(\hat{U}) = C_{\text{IP}}\frac{p^2}{h}\{\{G(f(\phi,\mu))\}\}\underline{[\![\hat{U}]\!]}. \tag{D3}
$$

In addition, it appears natural to symmetrize the diffusive part by

$$
-\int_0^T \int_{\Gamma_3} \{\{G(f(\phi,\mu))\nabla(P)\}\} : \underline{[\![\hat{U}]\!]}. \tag{D4}
$$

For the advective-flux, we can refer to upwinding as

$$
\{\{\phi F(U)\cdot\vec{n}\}\}_{Up} = \frac{1}{2}\left[\phi^+F(U^+)\cdot\vec{n} + \phi^-F(U^-)\cdot\vec{n}\right]. \tag{D5}
$$

Finally, a complete SIP-DG-scheme over $\mathcal{T}_h$ is obtained by allowing discontinuous cell-transitions, performing integration and integration by parts on each cell. If we allow alternation in the usage of the numerical flux function $\mathcal{F}$ we obtain the SIP-DG scheme in known form (58).

APPENDIX E. NUMERICAL CONVERGENCE OF THE SMOOTHED APPROACH

As mentioned in Section 4.2, the numerical scheme used to handle discontinuous sediment and porosity coefficients forms the limit of a smoothed scenario. We numerically justify this by relying the smoothed porosity on smoothed step functions in one dimension, that is, for discontinuities located at $x_0 < x_1 \in \mathbb{R}$ the smoothed porosity is obtained from

$$\phi_\alpha(x) = [1 - \psi(x, \alpha)]\, \phi_2 + \psi(x, \alpha), \tag{E1}$$

where

$$\psi(x,\alpha) = \begin{cases} 1, & \text{if } x \le x_0 - \alpha \wedge x \ge x_1 + \alpha, \\ -\frac{1}{4}\left(\frac{x_0 - x}{\alpha}\right)^3 + \frac{3}{4}\frac{x_0 - x}{\alpha} + \frac{1}{2}, & \text{if } x > x_0 - \alpha \wedge x < x_0 + \alpha, \\ 1 - \left(-\frac{1}{4}\left(\frac{x_1 - x}{\alpha}\right)^3 + \frac{3}{4}\frac{x_1 - x}{\alpha} + \frac{1}{2}\right), & \text{if } x > x_1 - \alpha \wedge x < x_1 + \alpha, \\ 0 & \text{if } x \ge x_0 + \alpha \wedge x \le x_1 - \alpha. \end{cases} \tag{E2}$$

We can observe exemplifications for varying α in Figure E1. We now define error norms for water height H and weighted velocity uH as

$$E_H = \|H - H_\alpha\| = \left(\int_0^T \int_\Omega (H - H_\alpha)^2 \, \mathrm{d}x \, \mathrm{d}t\right)^{1/2}, \tag{E3}$$

$$E_{uH} = \|uH - uH_\alpha\| = \left(\int_0^T \int_\Omega (uH - uH_\alpha)^2 \, \mathrm{d}x \, \mathrm{d}t\right)^{1/2}. \tag{E4}$$

From construction of the well-balanced scheme it is obvious that steady state conditions $uH = 0$ for $H + z = C$ lead to zero error norms. We hence exemplifying investigate Gaussian initial conditions for the surface height H, that is, $(H_0, uH_0) = (1 + 0.3\exp(-100(x - 1/2)^2), 0)$, for final time $T = 0.4$ and step size $dt = 1\mathrm{e} - 3$, where the discontinuities are located at

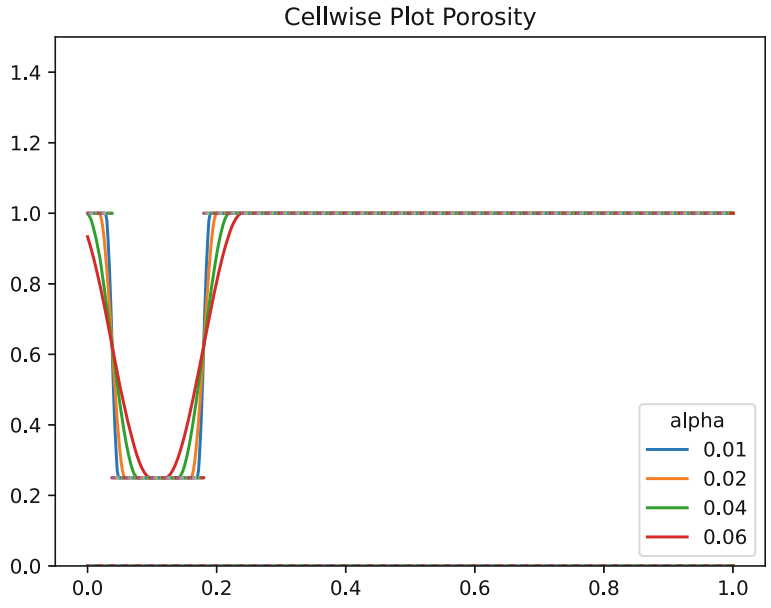

FIGURE E1 Smoothed porosity for $\alpha \in \{0.01, 0.02, 0.04, 0.06\}$

TABLE E1 Error norms E_H and E_{uH} for decreasing α

α	$\|H - H_\alpha\|$	$\|uH - uH_\alpha\|$
0.06	3.45587	8.41055
0.04	2.05134	4.69693
0.03	1.40056	3.08506
0.02	0.81980	1.69824
0.01	0.3443	0.601958
0.005	0.17583	0.23194
0.001	0.10549	0.11108

$x_0 = 0.038$ and $x_1 = 0.18$. We can observe the convergence numerically, that is, $U = \lim_{\alpha \to 0} U_\alpha$ for $\phi = \lim_{\alpha \to 0} \phi_\alpha$, as shown in Table E1. At this point, we would like to emphasize that the convergence is limited by the grid size of the mesh, hence showing the limit decrease for $\alpha \to 0$ is only possible for $h_\kappa \to 0$.